Variational approach to droplet transport via bendotaxis: Thin film dynamics and model reduction

Zhen Zhang [*]
Department of Mathematics, International Center for Mathematics, National Center for Applied Mathematics (Shenzhen), Guangdong Provincial Key Laboratory of Computational Science and Material Design, Southern University of Science and Technology 1088 Xueyuan Avenue, Shenzhen, PRC

Tiezheng Qian [†]
Department of Mathematics, The Hong Kong University of Science and Technology Clear Water Bay, Kowloon, Hong Kong, PRC

(Received 21 November 2021; accepted 31 March 2022; published 20 April 2022)

Bendotaxis has recently been theoretically proposed and experimentally observed by Bradley *et al.* [Phys. Rev. Lett. **122**, 074503 (2019)] as a mechanism for self-transport of droplets at small scales. As a result of the coupling between bending elasticity and capillarity in a thin channel, a pressure gradient is induced within a liquid droplet and leads to its spontaneous movement, regardless of whether the droplet is wetting or nonwetting the channel walls. In the present work, using Onsager's variational principle, we present a variational framework for systematically studying the mechanism of bendotaxis. We derive a full model for the thin film dynamics of bendotaxis with thermodynamical consistency. Based on the full model, we specify the conditions under which the simplified model used by Bradley *et al.* can be validated. Furthermore, we use Onsager's principle as a tool for approximation to derive a reduced model. This model reduction leads to a description for droplet self-transport using a few slow state variables by which a clear physical picture is presented for the mechanism of bendotaxis. The reduced model is validated by comparing its predictions with the numerical results from solving the full model. Finally, we investigate the mechanism of bendotaxis for active droplets capable of self-propelled motion. We find that wettability and activity can jointly operate to enhance or weaken the self-transport effect of bendotaxis, depending on the sign of wettability (hydrophobic or hydrophilic) and the sign of activity (contractile or extensile).

DOI: 10.1103/PhysRevFluids.7.044002

I. INTRODUCTION

Self-transport of droplets at small length scales have attracted increasing attention in material sciences and fluid mechanics, e.g., durotaxis, tensotaxis, and curvotaxis [1–3]. These transport mechanisms have a large potential to be utilized in developing new technological applications such as self-cleaning surfaces [4], antifogging [5], and hairy coating [6]. Recently, a novel mechanism called bendotaxis has been investigated for droplet transport at small scales both experimentally and numerically [7]. In this work, a passive droplet is sandwiched between two slender bendable plates with one end clamped and the other end free. As a result of the capillarity-induced bending of the plates, the droplet is transported toward the free end regardless of the wettability of the plate

[*]zhangz@sustech.edu.cn
[†]Corresponding author: maqian@ust.hk

surface. This transport mechanism establishes a connection between the bending elasticity of the plates and the directional motion of droplet, and opens up a new topic area in the study of wetting statics and dynamics on deformable substrates. Very recently, the effect of contact angle hysteresis on bendotaxis has been studied [8].

Wetting phenomena on deformable substrates have been extensively studied in recent years. Many interesting effects have been investigated, e.g., the formation of cusps at the contact line, the stick-slip motion of the contact line, the transition from Young's law to Neumann's law, etc. [9–20]. In most of these works, the focus is put on the static or quasistatic profiles of fluid interfaces, substrates, and contact lines. Physically, the dynamic wetting phenomena on deformable substrates are more challenging and interesting, and the recently reported mechanism, namely bendotaxis [7], is worth further investigation since it involves complex coupling between elasticity and hydrodynamics. In particular, this coupling is further complicated by the presence of moving contact lines, where various forces compete with each other with large magnitude in a small region.

The contact line is defined as the intersection of the fluid-fluid interface with the solid wall in immiscible two-phase flows. At equilibrium, the contact angle is determined by the interfacial tensions through Young's equation [21]. When one phase is displaced by the other along the wall, there is the moving contact line. A classical problem in continuum fluid dynamics is that the moving contact line is incompatible with the no-slip boundary condition because the latter leads to a nonintegrable singularity in viscous stress [22]. For decades, there have been many modeling and simulation works to elucidate and solve the contact line problem by using molecular dynamics, hybrid multiscale methods, diffuse-interface models, and hydrodynamic models [23,24].

Variational approaches based on thermodynamic principles have been widely and fruitfully used for deriving continuum dynamic models, and Onsager's variation principle has proved to be an effective and powerful tool in model derivation and reduction. As a fundamental principle in linear irreversible thermodynamics [25], Onsager's variational principle was originally formulated for isolated systems, and can be readily extended to a description of isothermal systems with constant temperature being maintained in space and time [26,27]. According to Onsager's principle, the time evolution of the state variables in an isothermal process can be obtained by minimizing an action called the Rayleighian, which is the sum of (i) the rate of change of the free energy and (ii) the dissipation function. Over the years, Onsager's variational principle and its variants have been extensively employed in deriving models for irreversible dissipative dynamics, e.g., multicomponent multiphase flows, crystal growth, contact line dynamics, thin film dynamics, and grain boundary migration [28–31]. More recently, because of its variational nature, Onsager's principle has been used as a tool for approximation and model reduction in describing and simplifying many complex phenomena in fluid mechanics and soft matter physics [32–34]. Another point worth mentioning is that Onsager's variational principle has been extended and applied to the dynamic modeling of active soft matter, e.g., suspensions of bacteria and aggregates of cells, where a large number of self-propelled units move in fluids or more complex environments [35–37].

The purpose of the present work is to present a variational modeling of bendotaxis that ensures thermodynamical consistency in the presence of various free energies and dissipation mechanisms. Under the lubrication approximation for thin films, we apply Onsager's principle to derive the whole system of governing equations including all the necessary boundary conditions. In our variational approach, all the free energies and dissipation mechanisms are included in the Rayleighian of the full model, and their dynamic effects are respectively manifested in the governing equations through the corresponding reversible and irreversible forces. Taking an appropriate limit of the model parameters, we recover a minimal model for bendotaxis that was discussed in Ref. [7]. Furthermore, we employ Onsager's principle as a tool for approximation to derive a reduced model. Using a reasonable ansatz for the shape of elastic beams, we obtain the reduced model system which consists of three ordinary differential equations (ODEs) for three representative state variables: the averaged height of the droplet, the position of the droplet, and the slope of the elastic beam. In particular, by taking the limit of small droplet volume, we can recover the asymptotic expression for the droplet velocity, which was originally given in Ref. [7]. While the same expression is obtained in

Ref. [7] and the present work, our analytical approach is different from that in Ref. [7]. Numerical results obtained by solving the full model are used to validate the asymptotic expression for the droplet velocity in the limit of small droplet volume.

In recent years, the study of active matter has drawn a lot of interests in soft matter research [35–37]. While the active force acting on one active particle is independent of another, with its direction determined by the moving particle itself, collective nonequilibrium phenomena are generated over long periods and on large scales. It has been reported that the active forces are able to collectively induce spontaneous directional transport of an active droplet [38–40]. Therefore it is interesting to investigate how the mechanism of bendotaxis operates on active droplets capable of self-propelled motion. In the present work, this situation is considered by using the extended version of Onsager's principle formulated for treating active matter systems [41]. By incorporating the work done by the active stress in the Rayleighian, we obtain a modified expression for the droplet velocity in the asymptotic limit of small droplet volume. Our results generalize the mechanism of bendotaxis to active droplets, showing that wettability and activity can jointly operate to enhance or weaken the self-transport effect of bendotaxis. For example, the effect is enhanced if a hydrophobic surface is combined with a contractile active stress, or a hydrophilic surface is combined with an extensile active stress. However, the effect is weakened if the combination of wettability and activity is the other way around. This may lead to potential applications in the design of self-transport systems.

The value and advantage of our variational approach are as follows: (i) It presents a variational framework to model the system of bendotaxis with all the free energies and dissipation mechanisms explicitly included in the Rayleighian for the full model of thin film dynamics. (ii) In the full model, the origin of each reversible or irreversible force can be found in the corresponding free energy or dissipation mechanism in the Rayleighian. (iii) Given the variational nature of the full model, the reduced model is derived by using Onsager's principle as a tool for approximation. (iv) The force balance and the separation of timescales are clearly revealed in the reduced model and present an insightful interpretation of the mechanism for droplet self-transport via bendotaxis. (v) The joint effect of wettability and activity can be investigated by using the extended version of Onsager's principle for active soft matter [41].

This paper is organized as follows. Section II presents the variational derivation of the full model for the thin film dynamics of bendotaxis using Onsager's principle. There is also a discussion on the conditions under which the full model can be simplified. Numerical simulation based on the full model is also provided. Section III focuses on the model reduction by using Onsager's principle as a tool for approximation. In the limit of small droplet volume, the asymptotic expression for the droplet velocity is obtained and then validated through a comparison with the numerical results from solving the full model. Section IV is a discussion on the mechanism of bendotaxis and the approximation underlying the asymptotic expression for the droplet motion. Section V investigates the joint effect of wettability and activity on the mechanism of bendotaxis by using the extended version of Onsager's principle formulated for treating active matter systems. The paper is concluded in Sec. VI with a few remarks.

II. A VARIATIONAL MODEL FOR THE THIN FILM DYNAMICS OF BENDOTAXIS

For simplicity, we consider bendotaxis in a two-dimensional setting, suitable for a droplet that is long enough in the third dimension.

We take the vertical wall as the z axis and the axis of mirror symmetry as the x axis. Using the mirror symmetry, we only need to consider the upper half of the system. The elastic beam (represented by a curve Γ) is horizontally clamped at $z = H_0$ on the wall, and the liquid droplet resides between $x = x_-$ and $x = x_+$. The deformation of the beam is very small, and hence its free end is approximately at $x = L$, where L is the length of the beam. The contact angle θ is in general a function of time. Here we take the hydrophobic case with $\theta > \frac{\pi}{2}$ to present the model derivation, with the understanding that the hydrophilic case can be treated similarly. A schematic illustration of the system is shown in Fig. 1.

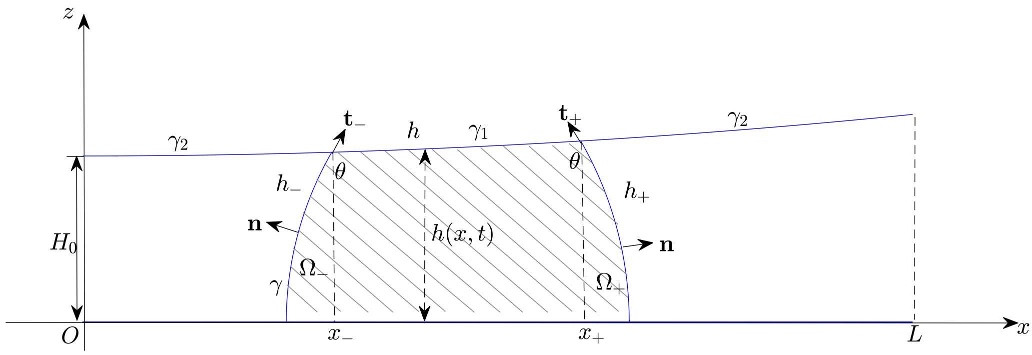

FIG. 1. A schematic illustration of the system in which the mechanism of bendotaxis works. Here the upper half of the system is shown ($z \geqslant 0$), and the beam surface is hydrophobic ($\cos\theta < 0$).

A. Onsager's variational principle

Onsager's variational principle is of fundamental importance to linear irreversible thermodynamics [25]. Below is an outline for its application to isothermal systems [26–28].

Consider an isothermal system that may include various boundaries. If the system deviates from its equilibrium state, then spontaneous processes will occur to bring the system back to equilibrium. In the linear response regime, the deviation from equilibrium is small and the time evolution of the system is slow, governed by the following variational principle. Let $\boldsymbol{\alpha}(t) = \{\alpha_1(t), \dots, \alpha_n(t)\}$ be a set of state variables to specify the macroscopic state. The time evolution of the system, given by the time derivatives of these variables $\dot{\boldsymbol{\alpha}}(t) = \{\dot{\alpha}_1(t), \dots, \dot{\alpha}_n(t)\}$, is determined by minimizing the following action (also called the Rayleighian) with respect to the rates $\{\dot{\alpha}_i\}$:

$$\mathcal{R}(\boldsymbol{\alpha}, \dot{\boldsymbol{\alpha}}) = \dot{F}(\boldsymbol{\alpha}, \dot{\boldsymbol{\alpha}}) + \Phi(\dot{\boldsymbol{\alpha}}, \dot{\boldsymbol{\alpha}}). \tag{1}$$

Here $F(\boldsymbol{\alpha}) := F(\alpha_1, \dots, \alpha_n)$ is the total free energy of the system, $\dot{F}$ is the rate of change of the total free energy, given by

$$\dot{F}(\boldsymbol{\alpha}, \dot{\boldsymbol{\alpha}}) = \sum_{i=1}^{n} \frac{\partial F}{\partial \alpha_i} \dot{\alpha}_i, \tag{2}$$

and $\Phi(\dot{\boldsymbol{\alpha}}, \dot{\boldsymbol{\alpha}})$ is the free-energy dissipation function which is defined as half the rate of free-energy dissipation. In the linear response regime, the dissipation function can be written as a quadratic function of the rates $\{\dot{\alpha}_i\}$:

$$\Phi(\dot{\boldsymbol{\alpha}}, \dot{\boldsymbol{\alpha}}) = \frac{1}{2} \sum_{i,j=1}^{n} \zeta_{ij} \dot{\alpha}_i \dot{\alpha}_j, \tag{3}$$

in which the friction coefficients ζ_{ij} form a symmetric and positive definite matrix. The symmetry of the ζ_{ij} matrix is based on the reciprocal relations which Onsager derived from the microscopic reversibility. Minimizing the Rayleighian with respect to the rates $\{\dot{\alpha}_i\}$ yields the kinetic equations

$$-\frac{\partial F}{\partial \alpha_i} - \sum_{j=1}^{n} \zeta_{ij} \dot{\alpha}_j = 0, \quad \text{for} \quad i = 1, \dots, n. \tag{4}$$

They express the force balance between the reversible force $-\frac{\partial F}{\partial \alpha_i}$ and the dissipative force $-\frac{\partial \Phi}{\partial \dot{\alpha}_i}$, which is linear in the rates $\{\dot{\alpha}_j\}$. Physically, the variational principle outlined above for isothermal systems can be derived from a more general variational principle based on the Onsager-Machlup action for nonisothermal systems.

When there are some nonconservative forces $f_i^{\mathrm{nc}}(\boldsymbol{\alpha}, t)$ (e.g., active forces) acting on the system, the rate of work done by these forces is

$$\dot{W}^{\mathrm{nc}}(\dot{\boldsymbol{\alpha}}, \boldsymbol{\alpha}) = \sum_{i=1}^{n} f_i^{\mathrm{nc}}(\boldsymbol{\alpha}, t)\dot{\alpha}_i, \tag{5}$$

and the evolution of the system is determined by minimizing the following Rayleighian with respect to the rates $\{\dot{\alpha}_i\}$:

$$\mathcal{R}(\boldsymbol{\alpha}, \dot{\boldsymbol{\alpha}}) = \dot{F}(\boldsymbol{\alpha}, \dot{\boldsymbol{\alpha}}) + \Phi(\dot{\boldsymbol{\alpha}}, \dot{\boldsymbol{\alpha}}) - \dot{W}^{\mathrm{nc}}(\dot{\boldsymbol{\alpha}}, \boldsymbol{\alpha}). \tag{6}$$

This leads to the kinetic equations

$$-\frac{\partial F}{\partial \alpha_i} - \sum_{j=1}^{n} \zeta_{ij}\dot{\alpha}_j + f_i^{\mathrm{nc}} = 0, \quad \text{for} \quad i = 1, \dots, n, \tag{7}$$

which still express the force balance. This extended version of Onsager's principle has been applied to model several active matter systems [41].

B. Free energies and dissipation functionals

The total free energy of the system consists of four components: the bending elastic energy F_b of the beam, the free energy of the solid-vapor interface F_{sv}, the free energy of the solid-liquid interface F_{sl}, and the free energy of the liquid-vapor interface F_{lv}.

The bending elastic energy is a special case of the Willmore energy, given by

$$F_b = \int_{\Gamma} \frac{1}{2} B\kappa^2 ds,$$

in which the Gaussian curvature is absent, B is the bending stiffness, κ is the curvature of the beam, and ds represents the arc length element. This energy is a special case of the Helfrich energy [42], which has been widely used in modeling membrane mechanics. Let $h(x, t)$ denote the height of the beam measured from $z = 0$ at the location x and the time t. Then the arc length element on Γ can be calculated as $ds = \sqrt{1 + (\frac{\partial h}{\partial x})^2}dx$ and the curvature of Γ is $\kappa = \frac{\frac{\partial^2 h}{\partial x^2}}{[1+(\frac{\partial h}{\partial x})^2]^{\frac{3}{2}}}$. In the limit of small deformation, the leading order terms are kept and the higher order terms are neglected, with the bending energy approximately given by

$$F_b = \int_0^L \frac{1}{2} B\left(\frac{\partial^2 h}{\partial x^2}\right)^2 dx. \tag{8}$$

As considered in Ref. [20], we assume that h is globally continuously differentiable, and is piecewise smooth with only two possibly nonsmooth points at $x = x_-$ and x_+.

In the small deformation limit, F_{sv} and F_{sl} can be expressed as [30]

$$F_{sl} = \int_{x_-}^{x_+} \gamma_1 \left[1 + \frac{1}{2}\left(\frac{\partial h}{\partial x}\right)^2\right] dx, \tag{9}$$

$$F_{sv} = \int_{x\in(0,x_-)\bigcup(x_+,L)} \gamma_2 \left[1 + \frac{1}{2}\left(\frac{\partial h}{\partial x}\right)^2\right] dx, \tag{10}$$

where γ_1 is the interfacial tension of the solid-liquid interface Γ_1, and γ_2 is the interfacial tension of the solid-vapor interface Γ_2. The (side part) liquid-vapor interfacial free energy is given by

$$F_{lv} = \int_{\Gamma_- \bigcup \Gamma_+} \gamma ds, \tag{11}$$

where γ is the liquid-vapor interfacial tension on $\Gamma_- \bigcup \Gamma_+$.

To apply Onsager's principle, it is necessary to understand the various dissipation mechanisms involved. In the present problem, the free energy is dissipated through the viscous dissipation in the liquid and the friction between the droplet and the beam. Under the lubrication approximation (with the droplet width $\Delta X = x_+ - x_-$ being much larger than the characteristic height H_0), the viscous dissipation functional can be written as

$$\Phi_v = \int_{x_-}^{x_+} \int_0^h \frac{\eta}{2}\left(\frac{\partial u}{\partial z}\right)^2 dz dx, \tag{12}$$

where u is the horizontal component of the velocity $\mathbf{u} = (u, w)$, and η is the shear viscosity of the liquid. Here a small fraction of volume in $\Omega_\pm$ is neglected. The boundary dissipation functional due to fluid slip on solid surface can be written as

$$\Phi_s = \int_{x_-}^{x_+} \frac{1}{2}\beta_s u^2 dx,$$

and the contact line dissipation function Φ_{CL} can be written as

$$\Phi_{\mathrm{CL}} = \frac{1}{2}\beta_{\mathrm{CL}}(\dot{x}_-^2 + \dot{x}_+^2),$$

where β_s is the friction coefficient on the beam surface and β_{CL} is that at the contact line.

Given the free energies and dissipation functionals supplemented with the incompressibility condition $\frac{\partial u}{\partial x} + \frac{\partial w}{\partial z} = 0$, we have all the components that will be used by Onsager's variational principle. The incompressibility condition can be imposed by introducing a constraint term

$$C = -\left(\int_{\Omega_- \bigcup \Omega_+} + \int_{x_-}^{x_+}\int_0^h\right) p\left(\frac{\partial u}{\partial x} + \frac{\partial w}{\partial z}\right) dz dx,$$

where p is a local Lagrange multiplier that can be interpreted as pressure.

C. Variational derivation of the system using Onsager's variational principle

The Rayleighian $\mathcal{R}$ is the sum of the time derivative of the total free energy $\dot{F}_b + \dot{F}_{sl} + \dot{F}_{sv} + \dot{F}_{lv}$, the total dissipation function $\Phi_v + \Phi_s + \Phi_{\mathrm{CL}}$, and the constraint term C. Direct calculation of the variations of $\mathcal{R}$ with respect to the generalized velocities (i.e., rates) in different domains will give the dynamic equations of the system. The derivation details are given in Appendix A.

In the leading order lubrication approximation, the thin film dynamics of bendotaxis is modeled by the system

$$\frac{\partial h}{\partial t} = \frac{\partial}{\partial x}\left[\left(B\frac{\partial^5 h}{\partial x^5} - \gamma_1\frac{\partial^3 h}{\partial x^3}\right)\left(\frac{1}{3\eta}h^3 + \frac{1}{\beta_s}h^2\right)\right], \quad x \in (x_-, x_+), \tag{13}$$

$$B\frac{\partial^4 h}{\partial x^4} = \gamma_2\frac{\partial^2 h}{\partial x^2}, \quad x \in (0, x_-)\bigcup(x_+, L). \tag{14}$$

The jump conditions at $x = x_\pm$ are given by

$$[\![h]\!] = \left[\!\!\left[\frac{\partial h}{\partial x}\right]\!\!\right] = \left[\!\!\left[\frac{\partial^2 h}{\partial x^2}\right]\!\!\right] = 0, \tag{15}$$

$$B\left[\!\!\left[\frac{\partial^3 h}{\partial x^3}\right]\!\!\right] \pm (\gamma_1 - \gamma_2)\frac{\partial h}{\partial x} + \gamma\sin\theta = 0, \tag{16}$$

$$B\left[\!\!\left[\frac{\partial^4 h}{\partial x^4}\right]\!\!\right] \pm (\gamma_1 - \gamma_2)\frac{\partial^2 h}{\partial x^2} = \pm\frac{\gamma\cos\theta}{h}. \tag{17}$$

Here we use the notations $[\![f]\!]_{y^-}^{y^+} = f(y^+) - f(y^-)$ to represent the jump of f at y from y^- to y^+ (denoted by $[\![f]\!]$ for short). The clamped and free boundary conditions are respectively given by

$$h(0,t) = H_0, \quad \frac{\partial h}{\partial x}(0,t) = 0, \quad \frac{\partial^2 h}{\partial x^2}(L,t) = 0, \quad B\frac{\partial^3 h}{\partial x^3}(L,t) = \gamma_2 \frac{\partial h}{\partial x}(L,t). \tag{18}$$

Based on the contact line friction, the contact line dynamics is governed by

$$\mp \beta_{\mathrm{CL}} \dot{x}_{\pm} = \gamma_1 - \gamma_2 + \gamma \cos\theta, \tag{19}$$

where θ is the (microscopic) dynamic contact angle which is a dynamic variable. Finally, since the viscous dissipation in $\Omega_{\pm}$ is neglected, the pressure p is constant in $\Omega_{\pm}$, and hence the two liquid-vapor interfaces are of circular shape. As a result, each of the two liquid-vapor interfaces can be determined by the contact angle θ, the contact line position x_- or x_+, and the height of the beam $h(x_-, t)$ or $h(x_+, t)$. In addition, the conservation of the liquid mass leads to the kinematic condition

$$\dot{x}_{\pm} = -B\left(\frac{\partial^5 h}{\partial x^5} - \frac{\gamma_1}{B}\frac{\partial^3 h}{\partial x^3}\right)\left(\frac{1}{3\eta}h^2 + \frac{1}{\beta_s}h\right). \tag{20}$$

It is worth pointing out that in general, the dynamic contact angle θ may deviate from the equilibrium angle $\theta_e = \arccos(\frac{\gamma_2 - \gamma_1}{\gamma})$. This means that the dynamic contact angle θ and the contact line position $x_{\pm}$ should be solved simultaneously through coupling Eq. (19) with Eq. (20) in the model system. When the contact line friction coefficient β_{CL} is very small and the droplet motion is very slow (as considered in the present work), θ can be approximated by the equilibrium contact angle θ_e, and the contact line position $x_{\pm}$ is updated by the kinematic condition Eq. (20). It is also worth mentioning that with the viscous dissipation in $\Omega_{\pm}$ being neglected, the liquid-vapor interfaces $\Gamma_{\pm}$ become circular, and the microscopic dynamic contact angle θ can be regarded as the apparent contact angle.

We would like to emphasize that for the sake of a clear, straightforward explanation of bendotaxis, the dissipation function has been simplified as follows. (i) The viscous dissipation in $\Omega_{\pm}$ has been neglected. Because the volume of $\Omega_{\pm}$ is small compared to the droplet size, the additional dissipation due to the presence of moving contact lines is dropped in this treatment. Physically, the viscous stress is very strong in the vicinity of a moving contact line, characterized by a partial-slip region accompanied by a large interfacial curvature near the contact line. A notable consequence of neglecting the viscous dissipation in $\Omega_{\pm}$ is that the liquid-vapor interfaces $\Gamma_{\pm}$ are circular and of constant curvature in space. (ii) In the application to bendotaxis, it is assumed that the contact-line friction is negligible, and the contact angle θ is approximated by its equilibrium value. We use the hydrodynamic model [43,44] to estimate the effect of the additional dissipation due to the moving contact lines. In addition to the viscous dissipation $2\Phi_v$ with Φ_v expressed in Eq. (12) under the lubrication approximation, the viscous dissipation due to the contact line at $x = x_-(t)$ is approximately given by $\eta\dot{x}_-^2(C + P\ln\frac{R}{r_c})$, where $C \approx 3$ is contributed by the core region, $P\ln\frac{R}{r_c}$, with $P \approx 2$, is contributed by the partial-slip region with a power-law slip profile, R represents the overall size of the system ($R \sim H_0$), and $r_c \approx 6l_s$ is the size of the core region with $l_s = \frac{\eta}{\beta_s}$ being the slip length. It can be shown that under the lubrication approximation, $2\Phi_v$ is approximately given by $\frac{3\eta\dot{x}_-^2(x_+ - x_-)}{H_0}$. Therefore, the total dissipation is the sum of $2\Phi_v \approx \frac{3\eta\dot{x}_-^2(x_+ - x_-)}{H_0}$, $2\eta\dot{x}_-^2(C + P\ln\frac{R}{r_c})$ due to the contact lines (with a factor of 2 for both the left and right contact lines), and $\beta_{\mathrm{CL}}(\dot{x}_-^2 + \dot{x}_+^2) \approx 2\beta_{\mathrm{CL}}\dot{x}_-^2$ due to the friction at the contact lines. These components of dissipation can be used to evaluate the relative importance of $2\Phi_v$, which is explicitly considered in the computational model. For example, for $\frac{x_+ - x_-}{H_0} \approx 50$, $\frac{R}{r_c} \approx 100$, we have $2\Phi_v \approx 150\eta\dot{x}_-^2$ and $2\eta\dot{x}_-^2(C + P\ln\frac{R}{r_c}) \approx 24\eta\dot{x}_-^2$. This estimation shows that $2\Phi_v$ can acquire a dominance if the length-to-height ratio $\frac{x_+ - x_-}{H_0}$ of the droplet is very large, and the outer cutoff for the partial-slip region R is not very large compared to the size of the core region $r_c \approx 6l_s$. The latter condition means that the solid surface is slippery, and the slip length l_s is large.

D. Approximation in the limit of large stiffness

The above system of equations can be expressed in a dimensionless form using the following scaling:

$$\tilde{h} = \frac{h}{H_0}, \quad \tilde{x} = \frac{x}{L}, \quad \tilde{t} = \frac{Ut}{L},$$

where U is a characteristic velocity of the liquid. We also introduce the bendocapillary length $L_c = \sqrt{\frac{B}{\gamma}}$, the ratio between interfacial tensions $\tilde{\gamma}_i = \frac{\gamma_i}{\gamma}$ $(i = 1, 2)$, the capillary number $\mathrm{Ca} = \frac{\eta U}{\gamma}$, and the slip length $l_s = \frac{\eta}{\beta_s}$.

In the limit of large stiffness, the beam deformation is small and $\frac{L}{L_c} \ll 1$. Under the lubrication approximation for the aspect ratio $A = \frac{L}{H_0} \gg 1$ (or more accurately $\frac{\Delta X}{H_0} \gg 1$ as the lubrication approximation is applied to the droplet of width $\Delta X = x_+ - x_-$), we can consider the distinguished limits $\frac{L}{L_c} \sim \frac{H_0}{L}$ and $\mathrm{Ca} \sim \frac{H_0}{L}$. The first distinguished limit $\frac{L}{L_c} \sim \frac{H_0}{L}$ guarantees that the wettability is important through Eq. (17) after nondimensionalization. Using typical values of the parameters in Ref. [7], we have $\frac{H_0}{\Delta X} \approx \frac{1}{29}$, $L_c \approx 46$ mm, and $\frac{\Delta X}{L_c} \approx \frac{1}{10}$, which confirm that the wettability is important to the mechanism of bendotaxis. Combined with the first distinguished limit, the second distinguished limit $\mathrm{Ca} \sim \frac{H_0}{L}$ means that we are interested in a certain characteristic timescale $\tau_c = \frac{L}{U} \sim \frac{\eta L^2}{\gamma H_0}$ in which the thin film evolution is important. In addition, we assume that the whole system lies in the hydrodynamic regime in which the viscous dissipation is dominant. Then the boundary dissipation due to slip and the contact line dissipation can be neglected, with $\frac{l_s}{H_0} \ll 1$ and $\frac{\beta_{\mathrm{CL}}}{\eta} \ll \frac{L}{H_0}$.

Under the above assumptions, the system of equations can be reduced to

$$\frac{\partial \tilde{h}}{\partial \tilde{t}} = \frac{1}{3\nu} \frac{\partial}{\partial \tilde{x}} \left(\tilde{h}^3 \frac{\partial^5 \tilde{h}}{\partial \tilde{x}^5} \right), \quad \text{in} \quad \tilde{x} \in (\tilde{x}_-, \tilde{x}_+), \tag{21a}$$

$$\frac{\partial^4 \tilde{h}}{\partial \tilde{x}^4} = 0, \quad \text{in} \quad \tilde{x} \in (0, \tilde{x}_-) \bigcup (\tilde{x}_+, 1), \tag{21b}$$

$$\tilde{h} = 1, \quad \frac{\partial \tilde{h}}{\partial \tilde{x}} = 0, \quad \text{at} \quad \tilde{x} = 0, \tag{21c}$$

$$\frac{\partial^3 \tilde{h}}{\partial \tilde{x}^3} = \frac{\partial^2 \tilde{h}}{\partial \tilde{x}^2} = 0, \quad \text{at} \quad \tilde{x} = 1, \tag{21d}$$

$$[\![\tilde{h}]\!] = \left[\!\!\left[\frac{\partial \tilde{h}}{\partial \tilde{x}}\right]\!\!\right] = \left[\!\!\left[\frac{\partial^2 \tilde{h}}{\partial \tilde{x}^2}\right]\!\!\right] = \left[\!\!\left[\frac{\partial^3 \tilde{h}}{\partial \tilde{x}^3}\right]\!\!\right] = 0, \quad \left[\!\!\left[\frac{\partial^4 \tilde{h}}{\partial \tilde{x}^4}\right]\!\!\right] = \pm \frac{\nu}{\mathrm{Ca}A} \frac{\cos\theta}{\tilde{h}}, \quad \text{at} \quad \tilde{x} = \tilde{x}_\pm, \tag{21e}$$

$$\dot{\tilde{x}}_\pm = -\frac{1}{3\nu} \tilde{h}^2 \frac{\partial^5 \tilde{h}}{\partial \tilde{x}^5}, \quad \text{at} \quad \tilde{x} = \tilde{x}_\pm. \tag{21f}$$

Here $\theta = \arccos(\frac{\gamma_2 - \gamma_1}{\gamma})$ is the equilibrium contact angle at $\tilde{x} = \tilde{x}_\pm$, and $\nu = \frac{\mathrm{Ca} L^5}{L_c^2 H_0^3}$ is introduced as the bendability parameter. Note that the aforementioned distinguished limits $\frac{L}{L_c} \sim \frac{H_0}{L}$ and $\mathrm{Ca} \sim \frac{H_0}{L}$ lead to $\mathrm{Ca}A = O(1)$ and $\nu = O(1)$. And this can be satisfied if we choose the timescale $\tau_c = \frac{\eta L^2}{|\gamma \cos\theta| H_0}$, which is exactly the timescale considered in Ref. [7]. The physical meaning of each equation may be outlined as follows. The first Eq. (21a) describes the thin film evolution driven by the beam elasticity, and the second Eq. (21b) describes the equilibrium profile of the beam controlled by the beam elasticity. Equation (21c) is the clamp boundary conditions at the clamped end, and Eq. (21d) states the force balance at the free end. There are five jump conditions in Eq. (21e): the two conditions involving the zeroth- and the first-order derivatives enforce the continuity and smoothness of the beam at the contact lines; the two conditions involving the second- and the third-order derivatives describe the torque balance and normal force balance at the contact lines; the last condition involving the fourth-order derivative means that the pressure jump (on the left-hand side) is balanced by the interfacial curvature force (on the right-hand side). Equation (21f) is the kinematic condition required by the mass conservation. Our variational derivation not only presents a complete model for thin film dynamics, but also specifies the conditions under which the system in Eq. (21) is obtained. It is noted that Eq. (21) is consistent with the fluid flow model and beam deflection model in Ref. [8].

E. Numerical simulation of the full model

We employ the numerical method described in Appendix B to solve the system of dimensionless Eqs. (21).

We consider two cases: (1) the droplet (fluid 1) is hydrophilic with $\theta = \frac{\pi}{3}$ and (2) the droplet is hydrophobic with $\theta = \frac{2\pi}{3}$. In the numerical simulation, we take $A = 10$ for the aspect ratio, $\mathrm{Ca} = 0.09$ for the capillary number, and $\nu = 1$ for the bendability. The droplet is initially positioned between $\tilde{x}_-(0) = 0.3$ and $\tilde{x}_+(0) = 0.7$. Figure 2 shows the time evolution of the beam profile and the movement of the droplet.

Given the mirror symmetry about $z = 0$, we only show the time evolution of the upper beam. As depicted in the upper row of Fig. 2, as soon as the droplet is introduced between the two initially parallel beams, the (upper) beam starts to bend downwards in the hydrophilic case or bend upwards in the hydrophobic case. This change of the beam shape results from a competition between the interfacial energy and the bending elastic energy. In either the hydrophilic or the hydrophobic case, the droplet moves continuously toward the right end of the beam at a very slow velocity. Eventually, it arrives at the right end. It is observed that the part of the beam in contact with the droplet (marked in red) is less bent than that between $\tilde{x} = 0$ and $\tilde{x}_-$.

Let us further consider the situation for droplets that are much smaller compared to the beam length. The droplet is initially positioned between $\tilde{x}_-(0) = 0.6$ and $\tilde{x}_+(0) = 0.7$. The lower row of Fig. 2 shows the time evolution of the beam profile and the movement of the small droplets, which are qualitatively similar to those of the large droplets. It is observed that the magnitude of bendotaxis decreases with the decreasing droplet size. The part of the beam in contact with the small droplet (marked in red) is almost a straight line segment. This gives us useful input for a reduced description of bendotaxis.

III. MODEL REDUCTION USING ONSAGER'S VARIATIONAL PRINCIPLE

In this section, we develop an approximate description of bendotaxis based upon Onsager's variational principle. For this purpose, the beam shape is approximated by piecewise polynomials: according to Eq. (21b) and the boundary conditions Eqs. (21c) and (21d), the left part of the beam in $[0, \tilde{x}_-]$ can be exactly solved as a cubic curve, and the right part of the beam in $[\tilde{x}_+, 1]$ can be solved as a straight line segment; furthermore, for a small droplet of $\Delta\tilde{X} = \tilde{x}_+ - \tilde{x}_- \ll 1$, the part of the beam in contact with the liquid droplet is approximately linear as indicated by the numerical results presented above. Hence, the regions $[\tilde{x}_-, \tilde{x}_+]$ and $[\tilde{x}_+, 1]$ can be described by one single linear function, in which $\tilde{h}$ and $\frac{\partial \tilde{h}}{\partial \tilde{x}}$ are continuous at $\tilde{x} = \tilde{x}_+$. In addition, $\tilde{h}$ and $\frac{\partial \tilde{h}}{\partial \tilde{x}}$ must be continuous at $\tilde{x} = \tilde{x}_-$ as well. This suggests an ansatz for the dimensionless height function of the beam

$$\tilde{h}(\tilde{x}, \tilde{t}) = \begin{cases} 1 + \left(\frac{\tilde{x}}{\tilde{x}_-}\right)^2 (3K_0^- - 3 - \tilde{x}_- K_1^-) + \left(\frac{\tilde{x}}{\tilde{x}_-}\right)^3 (\tilde{x}_- K_1^- - 2K_0^- + 2), & \tilde{x} \in [0, \tilde{x}_-]; \\ K_0^- + K_1^-(\tilde{x} - \tilde{x}_-), & \tilde{x} \in [\tilde{x}_-, 1], \end{cases} \tag{22}$$

in which $K_0^-(t) = \tilde{h}(\tilde{x}_-, \tilde{t})$, $K_1^-(t) = \frac{\partial \tilde{h}}{\partial \tilde{x}}(\tilde{x}_-, \tilde{t})$, and the continuity conditions for $\tilde{h}$ and $\frac{\partial \tilde{h}}{\partial \tilde{x}}$ at $\tilde{x} = \tilde{x}_-$ are satisfied. Note that $\tilde{h}(\tilde{x}, \tilde{t})$ involves only three free parameters, which are K_0^-, K_1^-, and $\tilde{x}_-$. Using

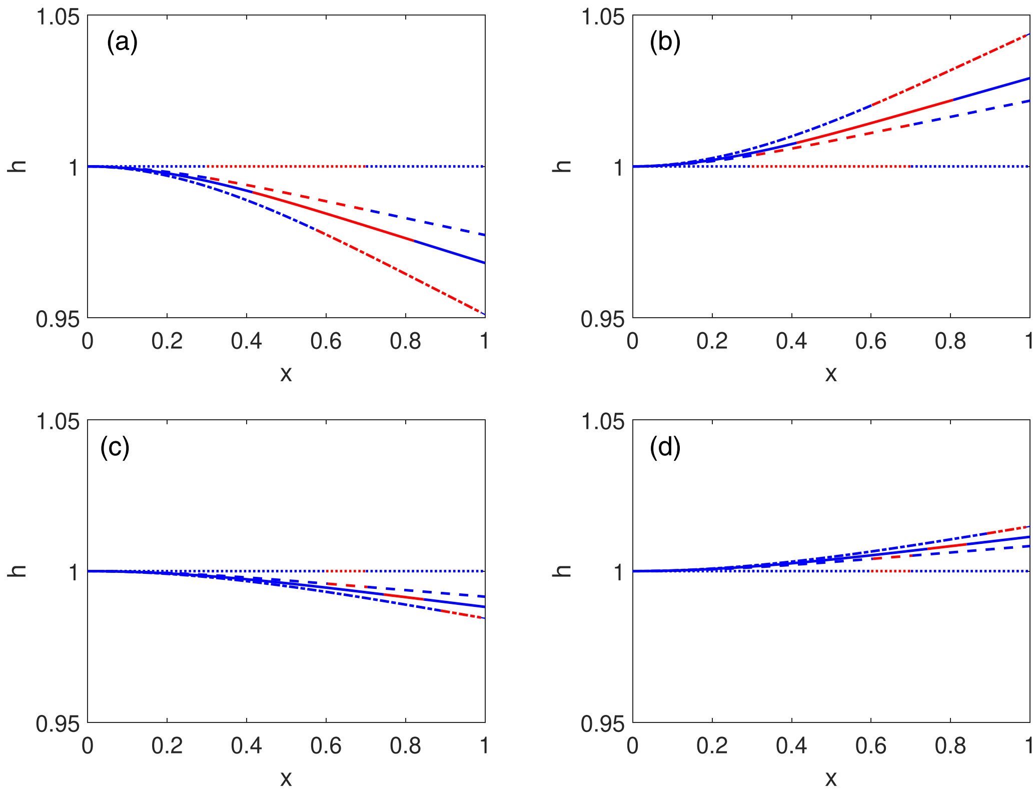

FIG. 2. Time evolution of the beam shown by its shape at four different stages: (a) initial stage (dotted), (b) bending stage (dashed), (c) moving stage (solid), and (d) final stage (dash-dotted). The part of the beam exposed to the air is marked in blue, while the part of the beam in contact with the liquid is marked in red. The upper row shows the results for a large droplet initially positioned between $x = 0.3$ and $x = 0.7$, while the lower row shows the results for a small droplet initially positioned between $x = 0.6$ and $x = 0.7$. The left column shows the results for hydrophilic droplets with $\theta = \frac{\pi}{3}$, while the right column shows the results for hydrophobic droplet with $\theta = \frac{2\pi}{3}$.

Onsager's variational principle, we will derive the dynamic equations governing the time evolution of these parameters.

A. Total free energy

The four components of free energy in Sec. II are made dimensionless using the reference energy γL. Using the approximate beam profile in Eq. (22), we obtain the corresponding dimensionless free energies as follows:

$$\tilde{F}_b = \frac{\mathrm{Ca}A}{\nu}\frac{1}{\tilde{x}_-^3}[6(K_0^- - 1)^2 - 6(K_0^- - 1)\tilde{x}_- K_1^- + 2(\tilde{x}_- K_1^-)^2],$$

$$\tilde{F}_{sl} = \frac{\gamma_1}{\gamma}(\tilde{x}_+ - \tilde{x}_-) + O\left(\frac{1}{A^2}\right),$$

$$\tilde{F}_{sv} = \frac{\gamma_2}{\gamma}(\tilde{x}_- - \tilde{x}_+ + 1) + O\left(\frac{1}{A^2}\right).$$

Again, it is obvious that the bending energy is important only if $\frac{\mathrm{Ca}A}{\nu} = O(1)$. Furthermore, for slow droplet motion, the capillary number is so small that the liquid-vapor interface always has enough time to relax to the quasiequilibrium profile. As a result, the left and right liquid-vapor interfaces are of circular shape with the radii $R_- = K_0^- H_0/|\cos\theta|$ and $R_+ = (K_0^- + K_1^- \Delta\tilde{X})H_0/|\cos\theta|$ respectively. The dimensionless liquid-vapor interfacial free energy is simply given by

$$\tilde{F}_{lv} = \frac{1}{\gamma L}\left[\gamma R_-\left(\theta - \frac{\pi}{2}\right) + \gamma R_+\left(\theta - \frac{\pi}{2}\right)\right] = O\left(\frac{1}{A}\right),$$

negligible in the thin film geometry.

Under the lubrication approximation for $A = \frac{L}{H_0} \gg 1$, we keep the dominant terms in the total free energy for variational analysis. Straightforward calculation shows that the rate of change of the total free energy is approximately given by

$$\begin{aligned}\dot{\tilde{F}}_{\text{tot}} = &-\frac{\text{Ca}A}{\nu}\frac{3\dot{\tilde{x}}_-}{\tilde{x}_-^4}[6(K_0^- - 1)^2 - 6(K_0^- - 1)\tilde{x}_- K_1^- + 2(\tilde{x}_- K_1^-)^2] \\ &+ \frac{\text{Ca}A}{\nu}\frac{1}{\tilde{x}_-^3}[(12K_0^- - 12 - 6\tilde{x}_- K_1^-)\dot{K}_0^- + (4\tilde{x}_- K_1^- - 6K_0^- + 6)(\dot{\tilde{x}}_- K_1^- + \tilde{x}_- \dot{K}_1^-)] \\ &+ \cos\theta(\dot{\tilde{x}}_- - \dot{\tilde{x}}_+),\end{aligned}$$

in which the contact angle θ is treated as a constant given by the equilibrium contact angle $\arccos\left(\frac{\gamma_2-\gamma_1}{\gamma}\right)$. This is an approximation valid for small droplets in slow motion.

B. Dissipation function

It is assumed that the boundary dissipation due to slip and the contact line dissipation on the beam surface can be neglected. To calculate the viscous dissipation in the liquid, we need the kinematic conditions (for mass conservation) in the droplet region $\tilde{x} \in [\tilde{x}_-, \tilde{x}_+]$:

$$\begin{aligned}&\frac{\partial\tilde{h}}{\partial\tilde{t}} + \frac{\partial(\tilde{h}\tilde{v})}{\partial\tilde{x}} = 0, \quad \tilde{x} \in (\tilde{x}_-, \tilde{x}_+), \\ &\tilde{v} = \dot{\tilde{x}}_- \quad \text{at} \quad \tilde{x} = \tilde{x}_-, \quad \text{and} \quad \tilde{v} = \dot{\tilde{x}}_+ \quad \text{at} \quad \tilde{x} = \tilde{x}_+,\end{aligned} \tag{23}$$

where $\tilde{v}(\tilde{x},\tilde{t}) = \frac{1}{\tilde{h}}\int_0^{\tilde{h}} \tilde{u}d\tilde{z}$ is the height averaged velocity. From these conditions, we obtain $\tilde{v}$ in the form of

$$\tilde{v} = \frac{1}{\tilde{h}}\left[K_0^-\dot{\tilde{x}}_- + (-\dot{K}_0^- + \dot{\tilde{x}}_- K_1^-)(\tilde{x} - \tilde{x}_-) - \frac{1}{2}\dot{K}_1^-(\tilde{x} - \tilde{x}_-)^2\right]. \tag{24}$$

It can be used to give $\tilde{v}$ at the right contact point $\tilde{x}_+$:

$$\dot{\tilde{x}}_+ = \frac{1}{\tilde{h}(\tilde{x}_+,\tilde{t})}\left[K_0^-\dot{\tilde{x}}_- + (-\dot{K}_0^- + \dot{\tilde{x}}_- K_1^-)(\Delta\tilde{X}) - \frac{1}{2}\dot{K}_1^-(\Delta\tilde{X})^2\right], \tag{25}$$

which is then used to further simplify the expression for $\dot{\tilde{F}}_{\text{tot}}$.

Using Eq. (A1) for the horizontal velocity component u and Eq. (A2) for the height averaged velocity $v(x,t)$ with the no-slip condition ($\beta_s \to \infty$), we can rewrite the viscous dissipation functional Eq. (12) as

$$\Phi_v = \int_{x_-}^{x_+} \frac{3\eta}{2h} v^2 dx. \tag{26}$$

Scaled by γU, Φ_v results in the dimensionless dissipation function

$$\tilde{\Phi} = \frac{3\text{Ca}A}{2}\int_0^{\Delta\tilde{X}} \frac{(K_0^-\dot{\tilde{x}}_- + (-\dot{K}_0^- + \dot{\tilde{x}}_- K_1^-)\xi - \frac{1}{2}\dot{K}_1^-\xi^2)^2}{(K_0^- + K_1^-\xi)^3} d\xi. \tag{27}$$

With $\dot{\tilde{F}}_{\text{tot}}$ and $\tilde{\Phi}$ ready, we will apply Onsager's variational principle below.

C. Variational derivation and asymptotic results

To apply Onsager's principle, we need to calculate the variations of the Rayleighian $\tilde{\mathcal{R}} = \dot{\tilde{F}}_{\text{tot}} + \tilde{\Phi}$ with respect to the rates of the three state variables $\dot{\tilde{x}}_-$, $\dot{K}_0^-$, and $\dot{K}_1^-$. Setting the corresponding variational derivatives to zero, we obtain a system of three ODEs:

$$\frac{\partial \tilde{\Phi}}{\partial \dot{\tilde{x}}_-} + \frac{\partial \dot{\tilde{F}}_{\text{tot}}}{\partial \dot{\tilde{x}}_-} = 0, \tag{28}$$

$$\frac{\partial \tilde{\Phi}}{\partial \dot{K}_0^-} + \frac{\partial \dot{\tilde{F}}_{\text{tot}}}{\partial \dot{K}_0^-} = 0, \tag{29}$$

$$\frac{\partial \tilde{\Phi}}{\partial \dot{K}_1^-} + \frac{\partial \dot{\tilde{F}}_{\text{tot}}}{\partial \dot{K}_1^-} = 0, \tag{30}$$

which govern the dynamics of the state variables $\tilde{x}_-$, K_0^-, and K_1^-.

For a small droplet of volume $\tilde{V} \ll 1$, we can asymptotically expand the above system of equations in terms of $\tilde{V}$. To be specific, we first obtain $\Delta\tilde{X} = \frac{1}{K_0^-}\tilde{V} + O(\tilde{V}^2)$ from the definition of $\tilde{V}$ in the limit of small volume $\tilde{V}$. Straightforward calculation shows that to the leading order of $O(\tilde{V})$, Eqs. (29) and (30) become

$$\frac{\text{Ca}A}{\nu}\frac{1}{\tilde{x}_-^3}(12K_0^- - 12 - 6\tilde{x}_-K_1^-) + \frac{\cos\theta}{(K_0^-)^2}\tilde{V} = 0, \tag{31}$$

$$\frac{\text{Ca}A}{\nu}\frac{1}{\tilde{x}_-^2}(4\tilde{x}_-K_1^- - 6K_0^- + 6) = 0, \tag{32}$$

from which we have $\tilde{x}_-K_1^- = \frac{3}{2}(K_0^- - 1) \sim O(\tilde{V})$. It is interesting to note that this equation ensures the continuity of $\frac{\partial^2\tilde{h}}{\partial\tilde{x}^2}$ at $\tilde{x} = \tilde{x}_-$. Letting $K_0^- - 1 = k_0^-\tilde{V} + O(\tilde{V}^2)$ and $K_1^- = k_1^-\tilde{V} + O(\tilde{V}^2)$, we obtain

$$k_0^- = -\frac{\nu}{3\text{Ca}A}\tilde{x}_-^3\cos\theta \quad \text{and} \quad k_1^- = \frac{3k_0^-}{2\tilde{x}_-}. \tag{33}$$

Keeping terms up to the order of $O(\tilde{V}^2)$, we can write Eq. (28) as

$$-\frac{\text{Ca}A}{\nu}\frac{9}{2\tilde{x}_-^4}(k_0^-)^2\tilde{V}^2 + 3\text{Ca}A\dot{\tilde{x}}_-\tilde{V} = 0, \tag{34}$$

from which we obtain the droplet velocity

$$\dot{\tilde{x}}_- = \frac{\nu}{6(\text{Ca}A)^2}\tilde{V}\tilde{x}_-^2\cos^2\theta, \tag{35}$$

which is in the order $O(\tilde{V})$, indicating that a small droplet moves slowly. Integrating this equation leads to an approximate expression for the contact line position $\tilde{x}_-$ as a function of time:

$$\tilde{x}_- = \frac{\tilde{x}_-(0)}{1 - \frac{\nu\tilde{x}_-(0)\tilde{V}\tilde{t}}{6(\text{Ca}A)^2}\cos^2\theta}, \tag{36}$$

which is valid for a droplet of small volume. Note that there is a factor $\cos^2\theta$ showing up in both Eqs. (35) and (36), which guarantees the unidirectional droplet motion regardless of the wettability condition (i.e., the sign of $\cos\theta$). We call it the bendotaxis factor.

The asymptotic results for $\tilde{x}_-$ are compared with the numerical results from the full model in Fig. 3 for both the hydrophilic ($\theta = 60^\circ$) and hydrophobic ($\theta = 120^\circ$) cases. The left panels show that the asymptotic results for $\tilde{x}_-$ are in good agreement with the full model results. It is noted that this agreement becomes less satisfactory as time goes by, and eventually the asymptotic expression Eq. (36) fails to predict the droplet motion since it blows up at $\tilde{t} = \frac{6(\text{Ca}A)^2}{\nu\tilde{x}_-(0)\tilde{V}\cos^2\theta}$. As depicted in the

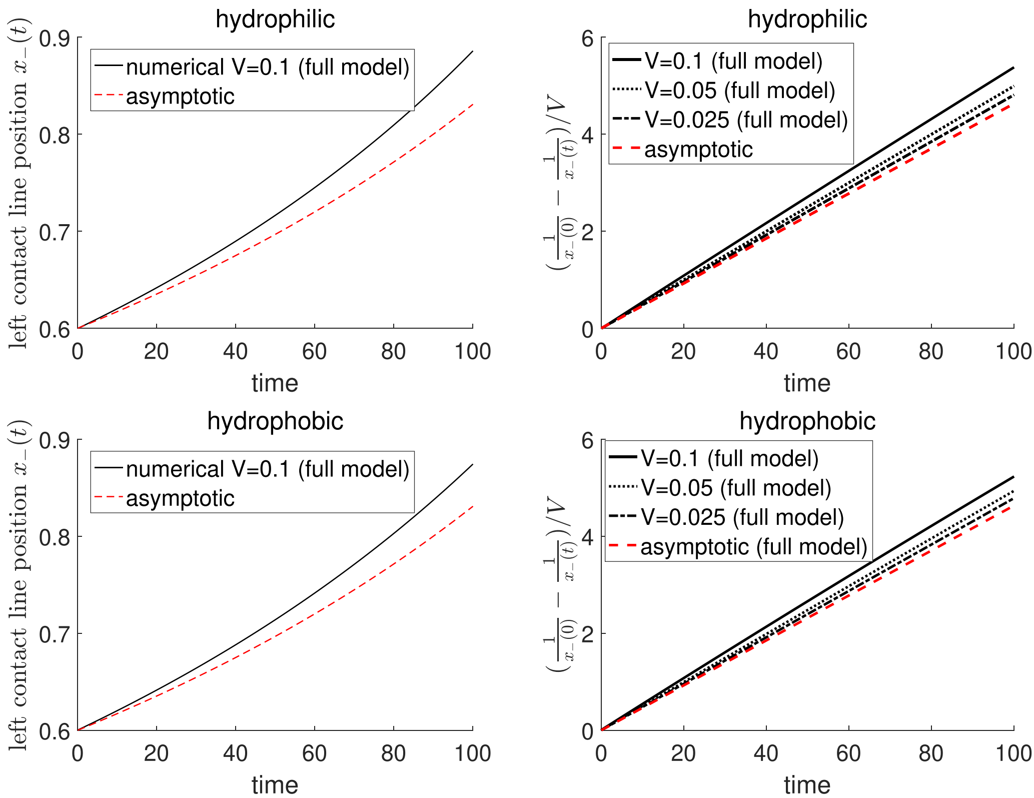

FIG. 3. The asymptotic results for the left contact line position $\tilde{x}_-(\tilde{t})$ are compared with the numerical results from the full model. The upper row is for the hydrophilic case with $\theta = \frac{\pi}{3}$, while the lower row is for the hydrophobic case with $\theta = \frac{2\pi}{3}$. The left column shows the contact line position $\tilde{x}_-$ as a function of $\tilde{t}$ for $\tilde{x}_-(0) = 0.6$, with the asymptotic results compared to the full model results for $\tilde{V} = 0.1$. The right column shows the convergence test for $(\frac{1}{\tilde{x}_-(0)} - \frac{1}{\tilde{x}_-(\tilde{t})})/\tilde{V}$. The full model results are computed for a diminishing set of values $\tilde{V} = 0.1$, 0.05, and 0.025. The red line is the asymptotic result given by $\frac{\nu\cos^2\theta}{6(\mathrm{Ca}A)^2}\tilde{t}$.

right panels, the quantity $(\frac{1}{\tilde{x}_-(0)} - \frac{1}{\tilde{x}_-(\tilde{t})})/\tilde{V}$ is linearly dependent on time. It is seen that the full model results approach the asymptotic value $\frac{\nu\cos^2\theta}{6(\mathrm{Ca}A)^2}$ as $\tilde{V}$ gets smaller. This confirms that the asymptotic results for droplet motion become more accurate for smaller droplet volume. It is also worth noting that the hydrophilic and hydrophobic cases show almost identical contact line motion, and hence verify the role of the bendotaxis factor $\cos^2\theta$ in Eqs. (35) and (36).

IV. DISCUSSION ON THE MECHANISM OF BENDOTAXIS

To better understand the mechanism of bendotaxis and the asymptotic expression for the droplet position Eq. (36), we start from the ansatz Eq. (22) for $\tilde{h}$ and the ad hoc condition $\frac{\partial^2\tilde{h}}{\partial\tilde{x}^2}(\tilde{x}_-, \tilde{t}) = 0$. This condition comes from the continuity of $\frac{\partial^2\tilde{h}}{\partial\tilde{x}^2}$ at $\tilde{x} = \tilde{x}_-$, a result expressed in Eq. (21e) from the full model. It leads to

$$\tilde{x}_- K_1^- = \tfrac{3}{2}(K_0^- - 1), \tag{37}$$

which has been derived in the asymptotic analysis to the order of $O(\tilde{V})$.

With the help of Eq. (37), we can write the approximate total free energy as

$$F_{\mathrm{tot}} \approx \frac{3BH_0^2}{2x_-^3}(K_0^- - 1)^2 - \gamma\cos\theta(x_+ - x_-)$$

in a dimensional form, up to an additive constant $\gamma_2 L$. The two free parameters involved in F_{tot} are K_0^- and x_-, with $K_0^- - 1$ measuring the vertical displacement of the beam at $x = x_-$ and x_- measuring the horizontal position of the droplet. The competition between the bending energy F_b ($\propto B$) and the interfacial energy F_γ ($\propto -\gamma\cos\theta$) indicates the existence of an optimal vertical displacement: a larger $K_0^- > 1$ means higher bending energy, while a smaller K_0^- leads to larger droplet width $x_+ - x_-$ due to mass conservation, and hence higher interfacial energy (for the hydrophobic case with $\cos\theta < 0$). Using a rectangle to approximate the droplet shape with $V \approx H_0 K_0^-(x_+ - x_-)$, we have

$$F_{\mathrm{tot}} = F_b + F_\gamma \approx \frac{3BH_0^2}{2x_-^3}(K_0^- - 1)^2 - \frac{V\gamma\cos\theta}{H_0 K_0^-}.$$

Since the relaxation of elastic deformation in the vertical direction is much faster than the droplet motion in the horizontal direction, it can be assumed that the vertical deformation of the beam is instantaneously optimized while the droplet moves. By considering the viscous dissipation caused by $\frac{dh}{dt}$ for $x \in (x_-, x_+)$ and combining it with F_{tot} which is a function of h at $x = x_-$, we can estimate the relaxation timescale τ_h for the vertical deformation of the beam. It can be shown that $\dot{x}_-\tau_h \ll x_+ - x_-$, with $\frac{\dot{x}_-\tau_h}{x_+ - x_-} \sim (\frac{x_-}{L})^5(\frac{x_+ - x_-}{L})^3 \ll 1$ for a small filling factor $\frac{x_+ - x_-}{L} \ll 1$. This means that the vertical deformation is much faster than the horizontal motion of the droplet. As a result, the vertical deformation is instantaneously equilibrated for a given droplet position. By minimizing F_{tot} w.r.t. K_0^-, we obtain the optimal vertical displacement, which is considered quasistatic while the droplet motion proceeds slowly. In the case of small deformation with $K_0^- - 1 = \epsilon \ll 1$, the elastic force due to the bending energy and the interfacial force due to the interfacial tensions are given by

$$-\frac{\partial F_b}{\partial \epsilon} \approx -\frac{3BH_0^2}{x_-^3}\epsilon, \tag{38}$$

$$-\frac{\partial F_\gamma}{\partial \epsilon} \approx -\frac{V\gamma\cos\theta}{H_0}. \tag{39}$$

The balance of these two forces minimizes the total free energy and gives

$$\epsilon \approx -\frac{x_-^3 V\gamma\cos\theta}{3BH_0^3}, \tag{40}$$

from which the quasistatic total free energy is approximately given by

$$F_{\mathrm{tot}} \approx -\frac{x_-^3 V^2\gamma^2\cos^2\theta}{6BH_0^4}.$$

As a result, the driving force for the droplet motion can be expressed as

$$-\frac{dF_{\mathrm{tot}}}{dx_-} \approx \frac{x_-^2 V^2\gamma^2\cos^2\theta}{2BH_0^4}. \tag{41}$$

It is worth pointing out that this driving force is just the integrated pressure difference acting on the droplet, in consistency with the mechanism proposed for bendotaxis [7]. In fact, the pressure on $\Gamma_\pm$ is $p(x_\pm, t) = -\frac{\gamma\cos\theta}{h(x_\pm, t)}$ for the hydrophobic case. A straightforward calculation shows that the integrated pressure difference is

$$
\begin{aligned}
[p(x_-,t)-p(x_+,t)]H_0 &= -\gamma\cos\theta\frac{H_0^2K_1^-(x_+-x_-)}{Lh(x_+,t)h(x_-,t)}\\
&\approx -\gamma\cos\theta\frac{3V(K_0^- -1)}{2H_0x_-}\\
&\approx\frac{x_-^2V^2\gamma^2\cos^2\theta}{2BH_0^4},
\end{aligned}
$$

in which Eqs. (37) and (40) have been used, with the droplet volume $V\approx H_0(x_+-x_-)$ for $\epsilon\ll 1$.

According to Onsager's variational principle, the driving force derived above should be balanced by the dissipative force caused by the viscous dissipation [in Eq. (26)]:

$$\Phi=\int_{x_-}^{x_+}\frac{3\eta}{2h}v^2dx\approx\frac{3\eta V\dot{x}_-^2}{2H_0^2}.$$

The force balance equation $-\frac{\partial F_{\rm tot}}{\partial x_-}-\frac{\partial\Phi}{\partial\dot{x}_-}=0$ gives the dimensional form of Eq. (35):

$$\dot{x}_-\approx\frac{x_-^2V\gamma^2\cos^2\theta}{6\eta BH_0^2}. \tag{42}$$

We remark that Eq. (42) for the droplet velocity is exactly the one found in Ref. [7], which was validated in comparison with experimental results. In the present work, we investigate the droplet dynamics by using variational and asymptotic analyses, which are more systematical and provide a straightforward physical picture as follows. It is the vertical force balance between the bending and interfacial forces [Eqs. (38) and (39)] that determines a quasistatic beam shape that gives rise to a horizontal force Eq. (41) to drive the droplet toward the free end.

We would like to point out that the mechanism of bendotaxis can be understood in terms of both energy and force. The total free energy can be approximately expressed as $F_{\rm tot}(x_-,h_-)=F_b(x_-,h_-)+F_\gamma(h_-)$, where the droplet position x_- and height h_- are treated as two independent variables, F_b is the bending energy, and F_γ is the interfacial energy, which is dominated by the interfacial energies at the solid-liquid and solid-vapor interfaces in the thin film geometry. The droplet is able to continuously lower the total free energy by moving toward the free end and pushing the beams further apart (for the hydrophobic case here). Due to the slow droplet motion in the horizontal direction, the vertical deformation is of a quasistatic nature, and the total free energy is minimized with respect to the vertical deformation, i.e., $-\frac{\partial F_{\rm tot}(x_-,h_-)}{\partial h_-}|_{h_-=h_e(x_-)}=0$, in which $h_-=h_e(x_-)$ is determined. This leads to

$$-\frac{dF_{\rm tot}[x_-,h_e(x_-)]}{dx_-}=-\frac{\partial F_{\rm tot}(x_-,h_-)}{\partial x_-}\bigg|_{h_-=h_e(x_-)}=-\frac{\partial F_b}{\partial x_-}\bigg|_{h_-=h_e(x_-)}$$

for the horizontal driving force, with $-\frac{\partial F_b}{\partial x_-}|_{h_-=h_e(x_-)}$ noted to be the horizontal component of the bending force due to the bending energy F_b. Perpendicular to the beam, the bending force is in the downward direction, balanced by the integrated liquid pressure, and given by $-\bar{p}(x_+-x_-)<0$, where $\bar{p}>0$ is the average pressure in the liquid. Using the average slope $[\frac{\partial h}{\partial x}]>0$ in the droplet region, we can write the positive horizontal component of the bending force as $\bar{p}(x_+-x_-)[\frac{\partial h}{\partial x}]=\bar{p}[h(x_+)-h(x_-)]$. As the pressure p at $x=x_\pm$ is given by $p=-\frac{\gamma\cos\theta}{h(x_\pm)}\propto h^{-1}$, we have $\bar{p}[h(x_+)-h(x_-)]=-[p(x_+)-p(x_-)]\bar{h}$, in which $[p(x_-)-p(x_+)]\bar{h}$ is the integrated Laplace pressure difference. Therefore, although our approach and that in Ref. [7] look ¡®different¡¯ in reasoning, the same result has been reached.

The hydrophilic case can be studied in a similar way, with the vertical displacement of the beam being negative while the droplet moves [from Eq. (40) with $\cos\theta>0$]. In short, the lower and upper

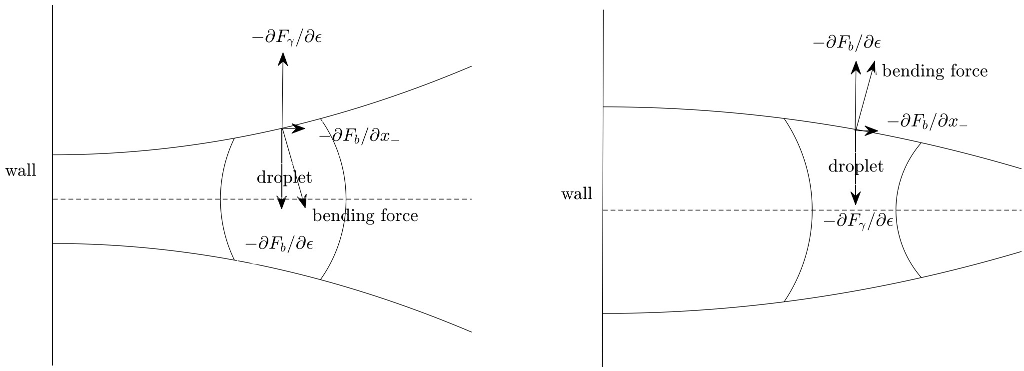

FIG. 4. A schematic illustration of the forces acting on the droplet. Left panel: In the hydrophobic case, the lower and upper beams are *pushed away from each other* by the droplet. As a result, the bending elastic force exerted by the upper beam on the droplet is *downward* pointing with a *positive* horizontal component. Right panel: In the hydrophilic case, the lower and upper beams are *pulled toward each other* by the droplet. As a result, the bending elastic force exerted by the upper beam on the droplet is *upward* pointing with a *positive* horizontal component. In either case, the vertical component of the bending elastic force is in balance with the interfacial force, and this vertical force balance determines the beam deformation, as expressed in Eqs. (38)–(40). The positive horizontal component of the bending elastic force, which is given by $-\frac{dF_{\rm tot}}{dx_-} = -\frac{\partial F_b}{\partial x_-}$ in Eq. (41), always drives the droplet to the right end.

beams are pushed away from each other by the droplet if the beam surface is hydrophobic, and they are pulled toward each other by the droplet if the beam surface is hydrophilic.

Here we add that as determined by the free-energy part of the system, there is a dependence of the driving force on the contact line position x_-, and hence the driving force increases with the increasing x_-. Meanwhile, even if the additional dissipation due to the contact lines are introduced, the dissipation function is still independent of x_- to the leading order in the reduced model. As a result, the droplet motion still accelerates as the channel end is approached. The additional dissipation, however, will change the dependence of the contact line velocity $\dot{x}_-$ on the droplet geometry.

Finally, the mechanism of bendotaxis can be summarized as follows. When the beam surface is hydrophobic with $\cos\theta < 0$, the droplet would shrink in the x direction to reduce the interfacial energy. Due to mass conservation, the droplet would extend in the vertical direction and push the lower and upper beams away from each other. Consequently, the droplet sandwiched between the two beams is *pushed inwards* by the deformed beams. In this case, Eq. (39) shows that the interfacial force due to the interfacial tensions has a positive vertical component that pushes up the upper beam, and Eq. (38) shows that the elastic force due to the bending energy has a negative vertical component (with $\epsilon > 0$) to balances the interfacial force, as illustrated in the left panel of Fig. 4. As a result, the upper beam tilts upwards (and the lower beam tilts downwards) with a small angle. This angle gives rise to a small, rightward horizontal component of the elastic force that *pushes* the droplet to the right end. The hydrophilic case with $\cos\theta > 0$ can be understood in a similar way, as illustrated in the right panel of Fig. 4. The physical picture outlined above explains why the droplet always moves to the free end regardless of the wetting property of the beam surface.

V. BENDOTAXIS FOR ACTIVE DROPLETS

In this section, we consider a generalized bendotaxis process in which the thin droplet is made of active fluid. The orientation vector field, denoted by $\mathbf{d} = (d_x, d_z)$, describes the average orientation of active agents inside the droplet. We assume that $\mathbf{d}$ is a unit vector, and the active filaments inside the droplet lack the head-tail polarity so that $\mathbf{d}$ and $-\mathbf{d}$ are equivalent. We also assume that the active filaments satisfy the planar anchoring condition on the beam surface. This means $\mathbf{d}$ is parallel to the local tangent of the beam surface, and hence

$$\mathbf{d} = \frac{1}{\sqrt{1+\left(\frac{\partial h}{\partial x}\right)^2}}\left(1, \frac{\partial h}{\partial x}\right), \quad \text{at} \quad z = h, \tag{43}$$

$$\mathbf{d} = (1, 0), \quad \text{at} \quad z = 0, \tag{44}$$

with the second boundary condition coming from the mirror symmetry about $z = 0$.

A. Free energy, active stress, and thin film dynamics

Under the lubrication approximation, the nematic elastic energy due to the orientational deformation is given by

$$F_d = \int_{x_-}^{x_+}\int_0^{h(x)} \frac{1}{2}k_d\left[\left(\frac{\partial d_x}{\partial z}\right)^2 + \left(\frac{\partial d_z}{\partial z}\right)^2\right]dzdx, \tag{45}$$

where k_d is the elastic constant. We will consider a simple case in which the orientation vector $\mathbf{d}$ varies slightly between the two given directions at $z = h$ and $z = 0$. Because of the small tilt angle $|\frac{\partial h}{\partial x}| \ll 1$, we have $|d_x| \gg |d_z|$. Differentiating $d_x^2 + d_z^2 = 1$ with respect to z leads to the identity $(\partial_z d_x)d_x + (\partial_z d_z)d_z = 0$. It follows that $|\partial_z d_x| \ll |\partial_z d_z|$, and hence $\frac{1}{2}k_d(\partial_z d_z)^2$ is dominant in Eq. (45).

Furthermore, we assume that the droplet motion due to bendotaxis is much slower in comparison to the relaxation of $\mathbf{d}$. This means that the orientation field reaches its quasiequilibrium state instantaneously while the droplet moves [38,39]. The quasistatic state of $\mathbf{d}$ is obtained by minimizing F_d in Eq. (45). Keeping its dominant term, we have the Euler-Lagrange equation

$$\frac{\partial^2 d_z}{\partial z^2} = 0, \tag{46}$$

subject to the boundary conditions at $z = 0$ and h. The solution is linear in z:

$$d_z = \frac{z}{h}\frac{\frac{\partial h}{\partial x}}{\sqrt{1+\left(\frac{\partial h}{\partial x}\right)^2}} = \frac{z}{h}\partial_x h + O\left(\frac{1}{A^3}\right), \tag{47}$$

and the first component is approximately constant:

$$d_x = \sqrt{1-d_z^2} = 1 + O\left(\frac{1}{A^2}\right). \tag{48}$$

The active character of the fluid is manifested through the active stress tensor

$$\boldsymbol{\sigma}_a = -\alpha\mathbf{d}\otimes\mathbf{d} = -\alpha\begin{pmatrix} 1 & \frac{z}{h}\partial_x h \\ \frac{z}{h}\partial_x h & 0\end{pmatrix} + O\left(\frac{\alpha}{A^2}\right), \tag{49}$$

where α is the activity parameter: the active stress is extensile if $\alpha > 0$ or contractile if $\alpha < 0$.

For fast relaxation of $\mathbf{d}$, the rate of work done by the active stress is given by

$$\dot{W}_a = -\int_{x_-(t)}^{x_+(t)}\int_0^{h(x,t)} \boldsymbol{\sigma}_a : \nabla\mathbf{u}dzdx \approx \int_{x_-(t)}^{x_+(t)}\int_0^{h(x,t)} \alpha\left(-\frac{\partial w}{\partial z} + \frac{z}{h}\frac{\partial h}{\partial x}\frac{\partial u}{\partial z}\right)dzdx \tag{50}$$

in which the lubrication approximation and the incompressibility condition $\frac{\partial u}{\partial x} + \frac{\partial w}{\partial z} = 0$ have been used.

Using integration by parts, the variation of the rate of work done by the active stress Eq. (50) can be expressed as

$$\delta\dot{W}_a = -\int_{x_-}^{x_+}\int_0^h \frac{\alpha}{h}\frac{\partial h}{\partial x}\delta u dz dx + \int_{x_-}^{x_+}\alpha(-\delta(\partial_t h) + \frac{\partial h}{\partial x}\delta u|_{z=h})dx,$$

where we have used the mirror symmetry $w|_{z=0} = 0$ and the kinematic condition $w|_{z=h} \approx \frac{\partial h}{\partial t}$. To model the thin film dynamics of active droplets, we apply Onsager's variational principle with the generalized Rayleighian $\mathcal{R}_a = \dot{F}_{\text{tot}} + \Phi - \dot{W}_a$. The procedure is similar to that for passive droplets (see Appendix A). For instance, the variations of $\mathcal{R}_a$ with respect to u and w in the droplet region $\{(x,z)|x_- \leqslant x \leqslant x_+, 0 \leqslant z \leqslant h\}$ lead to a modified Stokes equation with active force:

$$\frac{\partial p}{\partial x} - \eta\frac{\partial^2 u}{\partial z^2} + \frac{\alpha}{h}\frac{\partial h}{\partial x} = 0, \tag{51}$$

$$\frac{\partial p}{\partial z} = 0. \tag{52}$$

The variation of $\mathcal{R}_a$ with respect to u on Γ_1 still gives the Navier slip condition $\beta_s u = -\eta\frac{\partial u}{\partial z} + \alpha\frac{\partial h}{\partial x}$ at $z = h$, which includes an additional term due to the active stress. Furthermore, the variation of $\mathcal{R}_a$ with respect to $\partial_t h$ on Γ_1 gives the pressure

$$p(x,t) = B\frac{\partial^4 h}{\partial x^4} - \gamma_1\frac{\partial^2 h}{\partial x^2} + \alpha. \tag{53}$$

Using these equations, we can solve for the horizontal velocity component $u(x,z,t)$ and obtain the height averaged velocity

$$v(x,t) = -\frac{1}{3\eta}h^2\left(\frac{\partial p}{\partial x} + \frac{\alpha}{h}\frac{\partial h}{\partial x}\right) - \frac{\partial p}{\partial x}\frac{h}{\beta_s}. \tag{54}$$

For simplicity, we adopt the no-slip condition with $\beta_s \to +\infty$. Finally, using the conservation law $\frac{\partial h}{\partial t} + \frac{\partial(hv)}{\partial x} = 0$, we obtain the thin film equation for active droplets:

$$\frac{\partial h}{\partial t} = \frac{1}{3\eta}\frac{\partial}{\partial x}\left[\left(B\frac{\partial^5 h}{\partial x^5} - \gamma_1\frac{\partial^3 h}{\partial x^3} + \frac{\alpha}{h}\frac{\partial h}{\partial x}\right)h^3\right].$$

The other boundary and jump conditions are similar to those derived in the absence of activity. Under the same limiting conditions $\frac{L}{L_c} \sim \frac{H_0}{L} \ll 1$, $\text{Ca} \sim \frac{H_0}{L}$, $\frac{l_s}{H_0} \ll 1$ and $\frac{\beta_{\text{CL}}}{\eta} \ll \frac{L}{H_0}$, the dimensionless system of equations can be summarized as follows:

$$\frac{\partial\tilde{h}}{\partial\tilde{t}} = \frac{1}{3\nu}\frac{\partial}{\partial\tilde{x}}\left[\tilde{h}^3\left(\frac{\partial^5\tilde{h}}{\partial\tilde{x}^5} + \frac{\lambda\nu}{\text{Ca}A}\frac{1}{\tilde{h}}\frac{\partial\tilde{h}}{\partial\tilde{x}}\right)\right], \quad \text{in} \quad \tilde{x} \in (\tilde{x}_-, \tilde{x}_+), \tag{55a}$$

$$\frac{\partial^4\tilde{h}}{\partial\tilde{x}^4} = 0, \quad \text{in} \quad \tilde{x} \in (0, \tilde{x}_-)\bigcup(\tilde{x}_+, 1), \tag{55b}$$

$$\tilde{h} = 1, \quad \frac{\partial\tilde{h}}{\partial\tilde{x}} = 0, \quad \text{at} \quad \tilde{x} = 0, \tag{55c}$$

$$\frac{\partial^3\tilde{h}}{\partial\tilde{x}^3} = \frac{\partial^2\tilde{h}}{\partial\tilde{x}^2} = 0, \quad \text{at} \quad \tilde{x} = 1, \tag{55d}$$

$$[\![\tilde{h}]\!] = \left[\!\!\left[\frac{\partial\tilde{h}}{\partial\tilde{x}}\right]\!\!\right] = \left[\!\!\left[\frac{\partial^2\tilde{h}}{\partial\tilde{x}^2}\right]\!\!\right] = \left[\!\!\left[\frac{\partial^3\tilde{h}}{\partial\tilde{x}^3}\right]\!\!\right] = 0, \quad \left[\!\!\left[\frac{\partial^4\tilde{h}}{\partial\tilde{x}^4}\right]\!\!\right] = \pm\frac{\nu}{\text{Ca}A}\left(\frac{\cos\theta}{\tilde{h}} + \lambda\right), \quad \text{at} \quad \tilde{x} = \tilde{x}_\pm, \tag{55e}$$

$$\dot{\tilde{x}}_\pm = -\frac{1}{3\nu}\tilde{h}^2\left(\frac{\partial^5\tilde{h}}{\partial\tilde{x}^5} + \frac{\lambda\nu}{\text{Ca}A}\frac{1}{\tilde{h}}\frac{\partial\tilde{h}}{\partial\tilde{x}}\right), \quad \text{at} \quad \tilde{x} = \tilde{x}_\pm, \tag{55f}$$

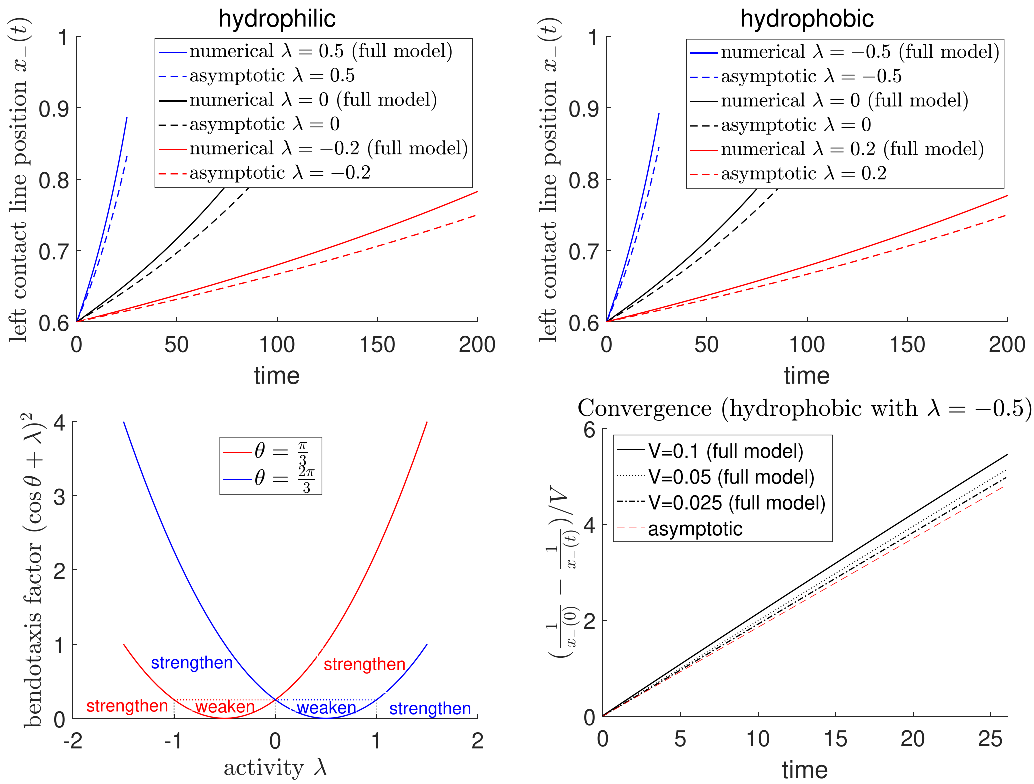

FIG. 5. The upper row shows the time evolution of the left contact point position $\tilde{x}_-$, computed from both the full model Eq. (55) and the asymptotic result in Eq. (61). The droplet is positioned between $\tilde{x}_-(0) = 0.6$ and $\tilde{x}_-(0) = 0.7$. Different activity parameters are considered for the hydrophilic case with $\theta = \frac{\pi}{3}$ (upper left) and the hydrophobic case with $\theta = \frac{2\pi}{3}$ (upper right). The lower left panel illustrates how the bendotaxis factor varies with the activity. The lower right panel shows the convergence test for $(\frac{1}{\tilde{x}_-(0)} - \frac{1}{\tilde{x}_-(\tilde{t})})/\tilde{V}$. Numerical results from the full model are computed for a diminishing set of values $\tilde{V} = 0.1$, 0.05, and 0.025. The red line is the asymptotic result given by $\frac{\nu(\cos\theta+\lambda)^2}{6(\mathrm{Ca}A)^2}\tilde{t}$.

where $\lambda = \frac{\alpha H_0}{\gamma}$ is the dimensionless activity. It is remarkable that the activity enters the system both in the thin film dynamics Eq. (55a) and the jump condition in the fourth-order derivative Eq. (55e). By introducing intermediate variables and treating the active terms implicitly, this linear system of equations can be numerically solved in a manner similar to that in Appendix B.

By solving the governing equations numerically, we obtain the time dependence of the left contact line position $\tilde{x}_-(t)$ for different combinations of wettability (measured by $\cos\theta$) and activity (measured by the dimensionless activity $\lambda = \frac{\alpha H_0}{\gamma}$). The results are shown in the upper row of Fig. 5, with comparison to the results obtained for the corresponding passive bendotaxis (with $\lambda = 0$). It is readily seen that some combination leads to strengthened bendotaxis (e.g., the combination of hydrophobicity and contractibility), and some other combination leads to weakened bendotaxis (e.g., the combination of hydrophilicity and contractibility). This will be explained by an asymptotic expression for droplet velocity that is to be derived in the next subsection.

B. Model reduction and asymptotic results for active droplets

We continue with the analysis in Sec. III to include the effect of active stress. Under the no-slip condition ($\beta_s \to \infty$), we can simplify the rate of active work Eq. (50) using the height averaged velocity Eq. (54). This is further normalized using γU, leading to the dimensionless form

$$\dot{\tilde{W}}_a = \lambda \int_{\tilde{x}_-}^{\tilde{x}_+} \tilde{h}\frac{\partial \tilde{v}}{\partial \tilde{x}} d\tilde{x}. \tag{56}$$

Using Eq. (22) for $\tilde{h}$ and Eq. (24) for $\tilde{v}$, we obtain $\dot{\tilde{W}}_a$ in the simplified form

$$\begin{aligned}\dot{\tilde{W}}_a = \lambda\bigg[&(-\dot{K}_0^- + \dot{\tilde{x}}_- K_1^-)\Delta\tilde{X} - \frac{1}{2}\dot{K}_1^-(\Delta\tilde{X})^2 \\ &- \int_0^{\Delta\tilde{X}} K_1^- \frac{K_0^-\dot{\tilde{x}}_- + (-\dot{K}_0^- + \dot{\tilde{x}}_- K_1^-)\xi - \frac{1}{2}\dot{K}_1^-\xi^2}{K_0^- + K_1^-\xi} d\xi\bigg],\end{aligned} \tag{57}$$

through an integration by parts. To obtain the governing equations in the presence of the active force, Onsager's variational principle is applied by minimizing the generalized Rayleighian $\tilde{\mathcal{R}}_a = \dot{\tilde{F}}_{\text{tot}} + \tilde{\Phi} - \dot{\tilde{W}}_a$ with respect to the rates $\dot{\tilde{x}}_-$, $\dot{K}_0^-$, and $\dot{K}_1^-$.

In the limit of small volume $\tilde{V} \ll 1$, the derivatives of $-\dot{\tilde{W}}_a$ with respect to $\dot{K}_0^-$, $\dot{K}_1^-$, and $\dot{\tilde{x}}_-$ can be asymptotically expressed as

$$-\frac{\partial \dot{\tilde{W}}_a}{\partial \dot{K}_0^-} = -\lambda\bigg[-\frac{1}{K_0^-}\tilde{V} + O(\tilde{V}^2)\bigg], \tag{58a}$$

$$-\frac{\partial \dot{\tilde{W}}_a}{\partial \dot{K}_1^-} = -\lambda\bigg[-\frac{1}{2(K_0^-)^2}\tilde{V}^2 + O(\tilde{V}^3)\bigg], \tag{58b}$$

$$-\frac{\partial \dot{\tilde{W}}_a}{\partial \dot{\tilde{x}}_-} = 0. \tag{58c}$$

Combining these with Eqs. (31), (32), and (34), we obtain

$$K_0^- = 1 + k_0^-\tilde{V} + O(\tilde{V}^2), \quad \text{with} \quad k_0^- = -\frac{\nu\tilde{x}_-^3}{3\text{Ca}A}(\cos\theta + \lambda), \tag{59}$$

$$K_1^- = k_1^-\tilde{V} + O(\tilde{V}^2), \quad \text{with} \quad k_1^- = \frac{3k_0^-}{2\tilde{x}_-}, \tag{60}$$

$$\dot{\tilde{x}}_- = \frac{\nu}{6(\text{Ca}A)^2}\tilde{V}\tilde{x}_-^2(\cos\theta + \lambda)^2 + O(\tilde{V}^2), \tag{61}$$

which describe the dynamics of bendotaxis for active droplets. In comparison with Eq. (35), we see that in Eq. (61) there is an active term λ due to the active stress. Moreover, the balance between Eq. (58a) and the reversible force $-\frac{\partial \dot{\tilde{F}}_{\text{tot}}}{\partial \dot{K}_0^-}$ in Eq. (29) to the leading order $O(\tilde{V})$ means that the active force drives the vertical displacement of the beam away from its quasistatic value in the passive bendotaxis ($\lambda = 0$). This leads to the new beam shape expressed in Eqs. (59) and (60). It is noted that the active force acting on the droplet has no horizontal component according to Eq. (58c). Physically, it is the active force, the bending elastic force, and the interfacial tension force in the vertical direction that jointly determine the quasistatic beam deformation. The deformed beam then gives rise to a horizontal component of the bending elastic force that pushes (or pulls) the droplet toward the free end. This is the mechanism of bendotaxis for active droplets. As shown in the lower left panel of Fig. 5, activity can be introduced to either strengthen or weaken the bendotaxis effect for both the hydrophilic and hydrophobic droplets. In particular, there is a value for the activity that can prevent bendotaxis from occurring, e.g., $\lambda = -0.5$ for the hydrophilic case and $\lambda = 0.5$ for the hydrophobic case.

In the lower right panel of Fig. 5, the predictions of the asymptotic expression Eq. (61) are compared to the numerical results from the thin film model, showing quantitative agreement for

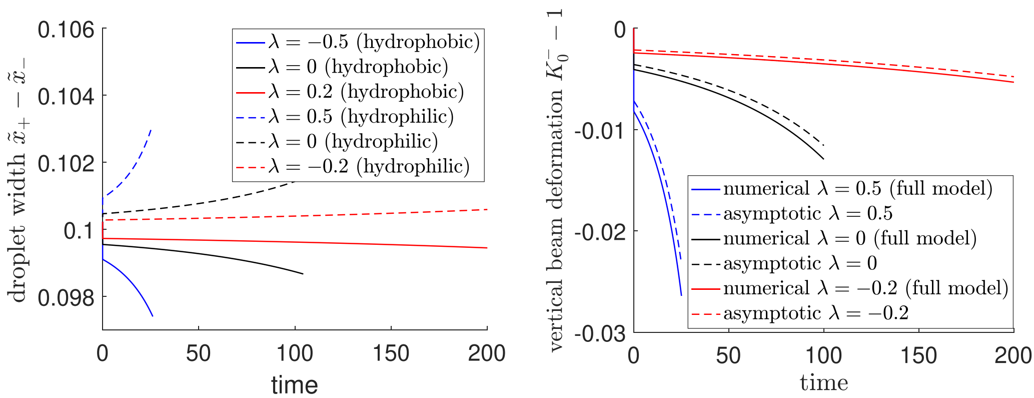

FIG. 6. The left panel shows the time evolution of droplet width $\tilde{x}_+ - \tilde{x}_-$, computed from the full model Eq. (55). The droplet is initially positioned between $\tilde{x}_-(0) = 0.6$ and $\tilde{x}_+(0) = 0.7$. Different activity parameters are considered for the hydrophilic and hydrophobic cases with $\theta = \frac{\pi}{3}$ and $\theta = \frac{2\pi}{3}$ respectively. The right panel shows the time evolution of beam deformation $K_0^- - 1$ for the hydrophilic case. The dashed lines represent the asymptotic result given by $-\frac{\nu \tilde{x}_-^3 \tilde{V}}{3\text{Ca}A}(\cos\theta + \lambda)$ in Eq. (59). It is observed that a very short transient time period is needed by the full model to establish the quasistatic state for vertical deformation.

small droplet volume. In Fig. 6, the time variations of droplet width and beam deformation are plotted.

C. More on the effect of active stress

Using the kinematic Eq. (23), the rate of work done by the active stress Eq. (56) can be rewritten as

$$\dot{\tilde{W}}_a = -\lambda \int_{\tilde{x}_-}^{\tilde{x}_+} \left(\frac{\partial \tilde{h}}{\partial \tilde{t}} + \tilde{v} \frac{\partial \tilde{h}}{\partial \tilde{x}} \right) d\tilde{x}, \tag{62}$$

which relates the average rate of change of the droplet height to the rate of active work. According to this expression for $\dot{\tilde{W}}_a$, the (dimensionless) active force acting on the droplet in the vertical direction is given by $-\lambda(\tilde{x}_+ - \tilde{x}_-)$, and its effect can be discussed for two different cases. If the active stress is contractile, i.e., $\lambda < 0$, then the droplet width tends to decrease in the horizontal direction, and hence the average droplet height tends to increase due to incompressibility. This height increase is a response to the positive active force acting on the droplet in the vertical direction. If the active stress is extensile, i.e., $\lambda > 0$, then the droplet width tends to increase in the horizontal direction, and hence the average droplet height tends to decrease due to incompressibility. This height decrease is a response to the negative active force acting on the droplet in the vertical direction. These phenomena caused by the active stress have been discussed in Ref. [40].

Based on the physical picture presented in Sec. IV, the wetting property of the beam surface and the active stress in the fluid jointly determine the quasistatic beam deformation in the vertical direction, and the bending elastic force exerted by the deformed beams push or pull the droplet toward the free end. According to Eq. (61), the coexistence of hydrophobicity ($\cos\theta < 0$) and contractibility ($\lambda < 0$) can mutually enhance the effect of bendotaxis. Similarly, the coexistence of hydrophilicity ($\cos\theta > 0$) and extensibility ($\lambda > 0$) can also mutually enhance the effect of bendotaxis. However, if the wetting parameter $\cos\theta$ and the activity parameter λ are of opposite signs, then the effect of bendotaxis will be weakened.

It is interesting to note that the droplet activity is manifested in the mechanism of bendotaxis through $(\cos\theta + \lambda)^2$ for which an explanation is given as follows. As presented in Sec. IV, the vertical deformation is quasistatic and can be determined from the total free energy

$F_{\rm tot}(x_-, h_-) = F_b(x_-, h_-) + F_\gamma(h_-)$, where the droplet position x_- and height h_- are treated as two independent variables, F_b is the bending energy, and F_γ is the interfacial energy. In the presence of droplet activity, the quasistatic nature of vertical deformation can be expressed through $-\frac{\partial F_{\rm tot}(x_-,h_-)}{\partial h_-}|_{h_-=h_e(x_-)} - \frac{\alpha V}{h_-}|_{h_-=h_e(x_-)} = 0$, in which $\frac{\alpha V}{h_-}$ is the active force acting on the droplet in the z direction, and $h_e(x_-)$ is the quasistatic height of the droplet at $x = x_-$. This gives the vertical deformation $h_e(x_-) - H_0 \propto \cos\theta + \lambda$. Note that in Fig. 6, the numerical results explicitly involve the factor of $\cos\theta + \lambda$. The horizontal driving force acting on the droplet can be expressed as

$$-\frac{\partial F_{\rm tot}(x_-, h_-)}{\partial x_-}\bigg|_{h_-=h_e(x_-)} + \left[-\frac{\partial F_{\rm tot}(x_-, h_-)}{\partial h_-}\bigg|_{h_-=h_e(x_-)} - \frac{\alpha V}{h_-}\bigg|_{h_-=h_e(x_-)}\right]\frac{dh_e(x_-)}{dx_-},$$

which becomes

$$-\frac{\partial F_{\rm tot}(x_-, h_-)}{\partial x_-}\bigg|_{h_-=h_e(x_-)}$$

for $h_- = h_e(x_-)$. As the dependence of $F_{\rm tot}$ on x_- comes from the bending energy $F_b(x_-, h_-)$ only, we obtain the horizontal driving force as $-\frac{\partial F_b(x_-,h_-)}{\partial x_-}|_{h_-=h_e(x_-)}$, which is proportional to $[h_e(x_-) - H_0]^2 \propto (\cos\theta + \lambda)^2$. Furthermore, the droplet activity does not change the dissipation function. It follows that the effect of droplet activity on bendotaxis is dependent upon $(\cos\theta + \lambda)^2$ and independent of the bendability ν.

VI. CONCLUSION

Using Onsager's variational principle, we have presented a variational approach to the modeling of bendotaxis. Under the lubrication approximation, we incorporate the Willmore elastic energy, the interfacial free energies, and the various dissipation mechanisms into the Rayleighian. We then derive the system of governing equations together with all the necessary boundary conditions. Based on the full model for the thin film dynamics of bendotaxis, we specify the limiting conditions under which the simplified model used in Ref. [7] can be validated.

We have also used Onsager's principle as a tool for approximation and model reduction. Using an ansatz in piecewise polynomial form for the beam shape, we derive a reduced model that involves only three slow state variables: the averaged height of the droplet, the position of the droplet, and the slope of the elastic beam. Taking the limit of small droplet volume, we asymptotically solve the system of three ODEs and obtain the leading order expression for the droplet velocity, in agreement with that originally presented in Ref. [7]. Numerical validation is made by comparing its predictions with the numerical results from solving the full model. Based on the variational analysis for the reduced model, we provide a clear physical picture for the mechanism of bendotaxis that involves a separation of timescales. In either the hydrophilic or hydrophobic case, the beam shape quickly relaxes to its quasistatic profile determined by the vertical force balance between the bending elastic force and the interfacial force. The slightly tilted beam then gives rise to a horizontal component of the bending elastic force by which the droplet is driven toward the free end.

Finally, we have considered bendotaxis for the self-transport of active droplets. Under the assumption of fast relaxation of the orientation field, we explicitly solve for the quasistatic orientation field and the corresponding active stress. Incorporating the work done by the active stress into Onsager's principle, we obtain the thin film model for active bendotaxis and the asymptotic equation for the self-transport of an active droplet via bendotaxis. It is found that the active stress affects the magnitude of bendotaxis by further changing the quasistatic beam shape. The interplay of the wettability and activity of the active droplet takes effect as follows: The self-transport via bendotaxis is enhanced if a hydrophobic surface is combined with a contractile active stress, or a hydrophilic surface is combined with an extensile active stress. However, if the combination of wettability and activity is the other way around, then the self-transport via bendotaxis is weakened.

In the present work, we have considered the self-transport via bendotaxis in a two-dimensional settings, which is a reasonable simplification for droplets that are long in the other dimension. If this is no longer the case, then the deformation of the elastic plates, rather than the beams, should be considered. As the plates may exhibit shapes that are more complex, the mechanism of bendotaxis can result in the self-transport of droplets in more complicated manner. Another complication comes from the contact line dynamics, which has been neglected in the present treatment. It may play an important role in the three-dimensional motion of droplets, especially at small length scales. In discussing the mechanism of bendotaxis for active droplets, we have not considered their self propulsion. Many experimental and theoretical results suggest that self propulsion may occur through symmetry breaking [45], and this effect may significantly affect self-transport processes via bendotaxis and some other mechanisms. Last but not the least, the control and optimization of self-transport processes, including those via bendotaxis, are very important in real-world applications, and their study require a combination of theoretical modeling and analysis, numerical simulation, and experimentation.

ACKNOWLEDGMENTS

The work of Z. Zhang was partially supported by the NSFC (Grants No. 11731006 and No. 12071207), the Guangdong Basic and Applied Basic Research Foundation (Grant No. 2021A1515010359), and the Guangdong Provincial Key Laboratory of Computational Science and Material Design (Grant No. 2019B030301001). The work of T. Qian was partially supported by the Hong Kong RGC grants (CRF No. C1006-20WF and GRF No. 16306121).

APPENDIX A: DERIVATION OF THIN FILM DYNAMICS FOR BENDOTAXIS

By dividing the integral Eq. (8) into three parts and applying integration by parts twice, we obtain the time derivative of F_b as

$$
\begin{aligned}
\dot{F}_b &= \left(\int_0^{x_-} + \int_{x_-}^{x_+} + \int_{x_+}^{L}\right) B\frac{\partial^2 h}{\partial x^2}\frac{\partial^2 \dot{h}}{\partial x^2}dx \\
&= B\frac{\partial^2 h}{\partial x^2}\frac{\partial \dot{h}}{\partial x}\bigg|_{x=L} - B\frac{\partial^3 h}{\partial x^3}\dot{h}\bigg|_{x=L} + B\frac{\partial \dot{h}}{\partial x}\bigg|_{x=x_-}\left[\!\!\left[\frac{\partial^2 h}{\partial x^2}\right]\!\!\right]_{x=x_-^+}^{x=x_-^-} + B\frac{\partial \dot{h}}{\partial x}\bigg|_{x=x_+}\left[\!\!\left[\frac{\partial^2 h}{\partial x^2}\right]\!\!\right]_{x=x_+^+}^{x=x_+^-} \\
&\quad + B\dot{h}(x_-,t)\left[\!\!\left[\frac{\partial^3 h}{\partial x^3}\right]\!\!\right]_{x=x_-^-}^{x=x_-^+} + B\dot{h}(x_+,t)\left[\!\!\left[\frac{\partial^3 h}{\partial x^3}\right]\!\!\right]_{x=x_+^-}^{x=x_+^+} + \left(\int_0^{x_-} + \int_{x_-}^{x_+} + \int_{x_+}^{L}\right) B\dot{h}\frac{\partial^4 h}{\partial x^4}dx,
\end{aligned}
$$

where we have used the clamp boundary conditions $h(0,t) = H_0$ and $\frac{\partial h}{\partial x}(0,t) = 0$, and the continuity of h and $\frac{\partial h}{\partial x}$ at $x = x_\pm$ to eliminate the corresponding boundary terms.

In a similar treatment with integration by parts, we obtain the time derivatives of F_{sl} and F_{sv} as

$$
\dot{F}_{sl} = \gamma_1\dot{h}\frac{\partial h}{\partial x}\bigg|_{x_-}^{x_+} - \int_{x_-}^{x_+}\gamma_1\dot{h}\frac{\partial^2 h}{\partial x^2}dx + \gamma_1\dot{x}_+\left[1 + \frac{1}{2}\left(\frac{\partial h}{\partial x}\right)^2\right]\bigg|_{x=x_+} - \gamma_1\dot{x}_-\left[1 + \frac{1}{2}\left(\frac{\partial h}{\partial x}\right)^2\right]\bigg|_{x=x_-},
$$

$$
\begin{aligned}
\dot{F}_{sv} &= \gamma_2\dot{h}\frac{\partial h}{\partial x}\bigg|_{x=L} - \gamma_2\dot{h}\frac{\partial h}{\partial x}\bigg|_{x_-}^{x_+} - \left(\int_0^{x_-} + \int_{x_+}^{L}\right)\gamma_2\dot{h}\frac{\partial^2 h}{\partial x^2}dx \\
&\quad - \gamma_2\dot{x}_+\left[1 + \frac{1}{2}\left(\frac{\partial h}{\partial x}\right)^2\right]\bigg|_{x=x_+} + \gamma_2\dot{x}_-\left[1 + \frac{1}{2}\left(\frac{\partial h}{\partial x}\right)^2\right]\bigg|_{x=x_-}.
\end{aligned}
$$

Finally, the liquid-vapor interfaces are denoted by $\Gamma_- = \{(x, h_-(x,t)) : x_-^0 \leqslant x \leqslant x_-\}$ and $\Gamma_+ = \{[x, h_+(x,t)] : x_+ \leqslant x \leqslant x_+^0\}$, with $x_\pm^0$ being the end of the curve $\Gamma_\pm$ at $z = 0$. A direct calculation using integration by parts yields

$$\frac{d}{dt}\int_{\Gamma_-}\gamma dl = -\int_{x_-^0}^{x_-}\frac{\gamma\frac{\partial^2 h_-}{\partial x^2}\dot{h}_-}{\left[1+\left(\frac{\partial h_-}{\partial x}\right)^2\right]^{\frac{3}{2}}}dx + \frac{\gamma\dot{x}_- + \gamma\frac{\partial h_-}{\partial x}\left(\frac{\partial h_-}{\partial t}+\dot{x}_-\frac{\partial h_-}{\partial x}\right)}{\sqrt{1+\left(\frac{\partial h_-}{\partial x}\right)^2}}\Bigg|_{x_-^0}^{x_-},$$

$$= -\int_{x_-^0}^{x_-}\gamma\kappa_-\dot{h}_- dx + \frac{\gamma\dot{x}_-}{\sqrt{1+\left[\frac{\partial h_-}{\partial x}(x_-,t)\right]^2}}$$

$$+\frac{\gamma\frac{\partial h_-}{\partial x}(x_-,t)}{\sqrt{1+\left[\frac{\partial h_-}{\partial x}(x_-,t)\right]^2}}\left[\frac{\partial h}{\partial t}(x_-,t)+\dot{x}_-\frac{\partial h}{\partial x}(x_-,t)\right],$$

where we have used the the boundary conditions $h_-(x_-^0,t)=0$ and $h_-(x_-,t)=h(x_-,t)$ (with their time derivatives), and the definition of the curvature $\kappa_- = \frac{\partial^2 h_-}{\partial x^2}[1+(\frac{\partial h_-}{\partial x})^2]^{-\frac{3}{2}}$ on Γ_-. The boundary term at x_-^0 vanishes due to the fact that $\frac{\partial h_-}{\partial t}(x_-^0,t)+\dot{x}_-^0\frac{\partial h_-}{\partial x}(x_-^0,t)=0$ and $\frac{\partial h_-}{\partial x}(x_-^0,t)=\infty$ as a result of the mirror symmetry at $z=0$. For small deformation of the beam, $\frac{\partial h}{\partial x}(x_-,t)$ is a small quantity and $\frac{\partial h_-}{\partial x}(x_-,t)=\tan(\pi-\theta)$. Then we have

$$\frac{d}{dt}\int_{\Gamma_-}\gamma dl = -\int_{x_-^0}^{x_-}\gamma\kappa_-\dot{h}_- dx - \gamma\dot{x}_-\cos\theta + \gamma\frac{\partial h}{\partial t}(x_-,t)\sin\theta.$$

Combining the above results for Γ_- and the similar results for Γ_+, we have the time derivative of F_{lv} as

$$\dot{F}_{lv} = -\int_{x_-^0}^{x_-}\gamma\kappa_-\dot{h}_- dx - \int_{x_+}^{x_+^0}\gamma\kappa_+\dot{h}_+ dx - \gamma\dot{x}_-\cos\theta + \gamma\frac{\partial h}{\partial t}(x_-,t)\sin\theta$$

$$+\gamma\dot{x}_+\cos\theta + \gamma\frac{\partial h}{\partial t}(x_+,t)\sin\theta,$$

where κ_+ is the curvature of Γ_+.

It is worth noting that the derivation of the time derivatives of the interfacial free energies F_{sl}, F_{sv}, and F_{lv} can be understood from the viewpoint of Reynolds transport theorem and integration by parts [46].

Using integration by parts, we obtain the variation of Φ_v as

$$\delta\Phi_v = -\int_{x_-}^{x_+}\int_0^h \eta\frac{\partial^2 u}{\partial z^2}\delta u dz dx + \int_{x_-}^{x_+}\eta\frac{\partial u}{\partial z}\delta u\Big|_{z=h},$$

where the mirror symmetry with $\frac{\partial u}{\partial z}=0$ at $z=0$ has been used to eliminate the boundary term at $z=0$. The variations of Φ_s and Φ_{CL} are easily obtained as

$$\delta\Phi_s = \int_{x_-}^{x_+}\beta_s u\delta u dx,$$

$$\delta\Phi_{\mathrm{CL}} = \beta_{\mathrm{CL}}(\dot{x}_-\delta\dot{x}_- + \dot{x}_+\delta\dot{x}_+).$$

The variation of the constraint term C is calculated using the divergence theorem:

$$\delta C = \left(\int_{x_-^0}^{x_-}\int_0^{h_-} + \int_{x_-}^{x_+}\int_0^{h} + \int_{x_+}^{x_+^0}\int_0^{h_+}\right)\left(\frac{\partial p}{\partial x}\delta u + \frac{\partial p}{\partial z}\delta w\right)dz dx$$

$$-\int_{\Gamma_-\bigcup\Gamma_+} p\delta v_n dl - \int_{\Gamma_{ls}} p\delta v_n dl$$

$$= \left(\int_{x_-^0}^{x_-} \int_0^{h_-} + \int_{x_-}^{x_+} \int_0^{h} + \int_{x_+}^{x_+^0} \int_0^{h_+} \right) \left(\frac{\partial p}{\partial x} \delta u + \frac{\partial p}{\partial z} \delta w \right) dz dx$$

$$- \int_{x_-^0}^{x_-} p\delta(\partial_t h_-) dx - \int_{x_+}^{x_+^0} p\delta(\partial_t h_+) dx - \int_{x_-}^{x_+} p\delta(\partial_t h) dx,$$

where the mirror symmetry with $w = 0$ at $z = 0$ is used to eliminate the boundary term at $z = 0$, and the kinematic condition $v_n = [1 + (\frac{\partial h}{\partial x})^2]^{-\frac{1}{2}} \frac{\partial h}{\partial t}$ is used to simplify the boundary term at $z = h$, plus similar treatment at $\Gamma_\pm$.

Setting $\frac{\delta \mathcal{R}}{\delta u} = 0$ and $\frac{\delta \mathcal{R}}{\delta w} = 0$ in the droplet regime $\{(x, z) | x_- \leqslant x \leqslant x_+, 0 \leqslant z \leqslant h\}$, we obtain

$$\frac{\partial p}{\partial x} - \eta \frac{\partial^2 u}{\partial z^2} = 0,$$

$$\frac{\partial p}{\partial z} = 0,$$

as the leading order Stokes equation in the lubrication approximation. It is readily seen that $p = p(x, t)$ is independent of z, and u is a quadratic function of z. Since $\Omega_\pm$ is much smaller compared to the whole droplet region, the viscous dissipation in $\Omega_\pm$ can be neglected, and hence p is constant in $\Omega_\pm$.

Now we focus on the boundary variations and the corresponding boundary conditions. Setting $\frac{\delta \mathcal{R}}{\delta u} = 0$ on Γ_1, we obtain the Navier slip boundary condition $\beta_s u = -\eta \frac{\partial u}{\partial z}$ at $z = h$. This leads to

$$u(x, z, t) = \frac{\partial_x p(x, t)}{2\eta} (z^2 - h^2) - \frac{\partial_x p(x, t)}{\beta_s} h, \tag{A1}$$

at $x \in (x_-, x_+)$, with the help of the mirror symmetry $\frac{\partial u}{\partial z} = 0$ at $z = 0$. Substituting Eq. (A1) into the height averaged velocity $v(x, t) = \frac{1}{h(x,t)} \int_0^{h(x,t)} u dz$, we obtain

$$v(x, t) = -\frac{\partial p}{\partial x} \left(\frac{1}{3\eta} h^2 + \frac{1}{\beta_s} h \right). \tag{A2}$$

Setting $\frac{\delta \mathcal{R}}{\delta(\partial_t h_\pm)} = 0$ on $\Gamma_\pm$ yields $p = -\gamma \kappa_\pm$. As p is constant in $\Omega_\pm$, $\kappa_\pm$ is constant along $\Gamma_\pm$ and can be expressed as $\kappa_\pm = \frac{\cos\theta}{h(x_\pm, t)}$ from a geometric consideration. Setting $\frac{\delta \mathcal{R}}{\delta(\partial_t h)} = 0$ on Γ_1, we obtain a force balance equation for the pressure in the liquid

$$p(x, t) = B \frac{\partial^4 h}{\partial x^4} - \gamma_1 \frac{\partial^2 h}{\partial x^2}, \tag{A3}$$

at $x \in (x_-, x_+)$. Substituting Eq. (A3) into Eq. (A2), we can express the conservation law $\frac{\partial h}{\partial t} + \frac{\partial (hv)}{\partial x} = 0$ as

$$\frac{\partial h}{\partial t} = \frac{\partial}{\partial x} \left[\left(B \frac{\partial^5 h}{\partial x^5} - \gamma_1 \frac{\partial^3 h}{\partial x^3} \right) \left(\frac{1}{3\eta} h^3 + \frac{1}{\beta_s} h^2 \right) \right].$$

Setting $\frac{\delta \mathcal{R}}{\delta(\partial_t h)} = 0$ at Γ_2, we obtain another force balance equation

$$B \frac{\partial^4 h}{\partial x^4} - \gamma_2 \frac{\partial^2 h}{\partial x^2} = 0, \tag{A4}$$

at $x \in (0, x_-) \bigcup (x_+, L)$ for part of the beam exposed to the vapor.

Finally, we consider the variations at the various boundaries. Setting $\frac{\delta \mathcal{R}}{\delta(\partial_t h)} = 0$ and $\frac{\delta \mathcal{R}}{\delta(\partial_{xt} h)} = 0$ at $x = L$, we have the free boundary conditions $B \frac{\partial^3 h}{\partial x^3} = \gamma_2 \frac{\partial h}{\partial x}$ and $B \frac{\partial^2 h}{\partial x^2} = 0$, which express the normal force balance and torque balance at $x = L$, respectively. Setting $\frac{\delta \mathcal{R}}{\delta(\partial_t h)} = 0$ and $\frac{\delta \mathcal{R}}{\delta(\partial_{xt} h)} = 0$ at $x = x_\pm$, we have the normal force balance and torque balance at the contact lines:

$$\pm(\gamma_1 - \gamma_2)\frac{\partial h}{\partial x} + B\left[\!\left[\frac{\partial^3 h}{\partial x^3}\right]\!\right] + \gamma \sin\theta = 0, \tag{A5}$$

$$B\left[\!\left[\frac{\partial^2 h}{\partial x^2}\right]\!\right] = 0. \tag{A6}$$

Combining Eqs. (A3), (A4), (A6), and the expression for the constant pressure $p = -\gamma\kappa_\pm = -\gamma\frac{\cos\theta}{h(x_\pm,t)}$ in $\Omega_\pm$, we obtain the jump condition for the fourth-order derivative of h at $x = x_\pm$:

$$B\left[\!\left[\frac{\partial^4 h}{\partial x^4}\right]\!\right] \pm (\gamma_1 - \gamma_2)\frac{\partial^2 h}{\partial x^2} = \pm\frac{\gamma\cos\theta}{h}. \tag{A7}$$

Setting $\frac{\delta \mathcal{R}}{\delta \dot{x}_\pm} = 0$, we have the tangential force balance at the contact lines:

$$\mp\beta_{\mathrm{CL}}\dot{x}_\pm = \gamma_1 - \gamma_2 + \gamma\cos\theta,$$

in which the high order term of $(\frac{\partial h}{\partial x})^2$ has been dropped.

From the mass conservation of liquid, we have the kinematic condition $\dot{x}_\pm = v(x_\pm)$ on $\Gamma_\pm$, i.e.,

$$\dot{x}_\pm = -\frac{B}{3\eta}\left(\frac{\partial^5 h}{\partial x^5} - \frac{\gamma_1}{B}\frac{\partial^3 h}{\partial x^3}\right)\left(h^2 + \frac{3\eta}{\beta_s}h\right).$$

APPENDIX B: NUMERICAL SCHEME

The system of dimensionless Eqs. (21) can be solved by using a finite difference scheme.

It is worth mentioning that the shape of the beam described by Eq. (21b) with the boundary conditions Eqs. (21c) and (21d) can be obtained as

$$\tilde{h}(\tilde{x},\tilde{t}) = \begin{cases} 1 + \left(\frac{\tilde{x}}{\tilde{x}_-}\right)^2(3K_0^- - 3 - \tilde{x}_- K_1^-) + \left(\frac{\tilde{x}}{\tilde{x}_-}\right)^3(\tilde{x}_- K_1^- - 2K_0^- + 2), & \tilde{x} \in [0, \tilde{x}_-]; \\ K_0^+ + K_1^+(\tilde{x} - \tilde{x}_+), & \tilde{x} \in [\tilde{x}_+, 1], \end{cases} \tag{B1}$$

in which $K_0^\pm(\tilde{t}) = h(\tilde{x}_\pm, \tilde{t})$ and $K_1^\pm(\tilde{t}) = \frac{\partial \tilde{h}}{\partial \tilde{x}}(\tilde{x}_\pm, \tilde{t})$.

To solve Eq. (21a), it is natural to introduce the transformation $\tilde{x} = \tilde{x}_- + (\tilde{x}_+ - \tilde{x}_-)f(\xi)$, with f being a smooth bijection from [0,1] to [0,1]. For simplicity, we choose $f(\xi) = \xi$. Under this transformation, the first equation in Eq. (21) is rewritten as

$$\frac{\partial \tilde{h}}{\partial \tilde{t}} - \frac{(1-\xi)\dot{\tilde{x}}_- + \xi\dot{\tilde{x}}_+}{\Delta\tilde{X}}\frac{\partial \tilde{h}}{\partial \xi} - \frac{1}{3\nu}\frac{1}{\Delta\tilde{X}}\frac{\partial}{\partial \xi}\left\{\frac{1}{(\Delta\tilde{X})^5}\frac{\partial^5 \tilde{h}}{\partial \xi^5}\tilde{h}^3\right\} = 0, \tag{B2}$$

with $\Delta\tilde{X} = \tilde{x}_+ - \tilde{x}_-$ and $\nu = \frac{\mathrm{Ca}L^5}{H_0^3 L_c^2}$.

Before discretizing this equation, it is helpful to recast the equation by introducing two intermediate variables:

$$\mu = \frac{\partial^2 \kappa}{\partial \tilde{x}^2} = \frac{1}{(\Delta\tilde{X})^2}\frac{\partial^2 \kappa}{\partial \xi^2}, \tag{B3}$$

$$\kappa = \frac{\partial^2 \tilde{h}}{\partial \tilde{x}^2} = \frac{1}{(\Delta\tilde{X})^2}\frac{\partial^2 \tilde{h}}{\partial \xi^2}. \tag{B4}$$

Then Eq. (B2) is recast as

$$\frac{\partial \tilde{h}}{\partial \tilde{t}} - \frac{(1-\xi)\dot{\tilde{x}}_- + \xi\dot{\tilde{x}}_+}{\Delta\tilde{X}}\frac{\partial \tilde{h}}{\partial \xi} - \frac{1}{3\nu}\frac{1}{\Delta\tilde{X}}\frac{\partial}{\partial \xi}\left(\frac{\tilde{h}^3}{\Delta\tilde{X}}\frac{\partial \mu}{\partial \xi}\right) = 0, \tag{B5}$$

Equations (B3), (B4), and (B5) form a system of second-order equations in the unknowns $\tilde{h}$, κ and μ. The boundary conditions are given by

$$\tilde{h}(\tilde{x}_-,\tilde{t}) = K_0^-, \quad \tilde{h}(\tilde{x}_+,\tilde{t}) = K_0^+,$$

$$\left.\frac{\partial \tilde{h}}{\partial \xi}\right|_{\tilde{x}_-} = K_1^- \Delta\tilde{X}, \quad \left.\frac{\partial \tilde{h}}{\partial \xi}\right|_{\tilde{x}_+} = K_1^+ \Delta\tilde{X},$$

$$\kappa(\tilde{x}_-,\tilde{t}) = \frac{6(1-K_0^-)+4\tilde{x}_-K_1^-}{(\tilde{x}_-)^2}, \quad \kappa(\tilde{x}_+,\tilde{t}) = 0,$$

$$\left.\frac{\partial \kappa}{\partial \xi}\right|_{\tilde{x}_-} = \frac{12(1-K_0^-)+6\tilde{x}_-K_1^-}{(\tilde{x}_-)^3}\Delta X, \quad \left.\frac{\partial \kappa}{\partial \xi}\right|_{\tilde{x}_+} = 0,$$

$$\mu(\tilde{x}_-,\tilde{t}) = -\frac{\nu}{\mathrm{Ca}A}\frac{\cos\theta}{K_0^-}, \quad \mu(\tilde{x}_+,\tilde{t}) = -\frac{\nu}{\mathrm{Ca}A}\frac{\cos\theta}{K_0^+},$$

$$-\frac{\tilde{h}^2(\tilde{x}_-,\tilde{t})}{3\nu(\Delta\tilde{X})}\left.\frac{\partial \mu}{\partial \xi}\right|_{\tilde{x}_-} = \dot{\tilde{x}}_-, \quad -\frac{\tilde{h}^2(\tilde{x}_+,\tilde{t})}{3\nu(\Delta\tilde{X})}\left.\frac{\partial \mu}{\partial \xi}\right|_{\tilde{x}_+} = \dot{\tilde{x}}_+.$$

We solve the system of Eqs. (B3)–(B5) using an implicit finite difference scheme. We divide [0, 1] into N equal subintervals and let the grid points be defined at the midpoint of each interval, i.e., $\xi_{i+\frac{1}{2}} = (i+\frac{1}{2})\Delta\xi$ for $i = 0,\dots,N-1$, where $\Delta\xi = \frac{1}{N}$. Let Δt be the time step, and $\tilde{h}^n_{i+\frac{1}{2}}$, $\kappa^n_{i+\frac{1}{2}}$, $\mu^n_{i+\frac{1}{2}}$ be approximations of $\tilde{h}(\xi_{i+\frac{1}{2}},\tilde{t}_n)$, $\kappa(\xi_{i+\frac{1}{2}},\tilde{t}_n)$, $\mu(\xi_{i+\frac{1}{2}},t_n)$ respectively. In practice, it is useful to introduce $V^n_{i+\frac{1}{2}} = (\tilde{x}^n_+ - \tilde{x}^n_-)\tilde{h}^n_{i+\frac{1}{2}}$ to preserve the volume conservation. Then the finite difference scheme is given by

$$\begin{aligned}
&\frac{V^{n+1}_{i+\frac{1}{2}} - V^n_{i+\frac{1}{2}}}{\Delta t} - \frac{\left(\frac{V^n_{i+\frac{3}{2}}+V^n_{i+\frac{1}{2}}}{2}\right)^3\left(\mu^{n+1}_{i+\frac{3}{2}}-\mu^{n+1}_{i+\frac{1}{2}}\right) - \left(\frac{V^n_{i+\frac{1}{2}}+V^n_{i-\frac{1}{2}}}{2}\right)^3\left(\mu^{n+1}_{i+\frac{1}{2}}-\mu^{n+1}_{i-\frac{1}{2}}\right)}{3\nu(\tilde{x}^n_+-\tilde{x}^n_-)^4(\Delta\xi)^2}\\
&-\frac{\left((1-\xi_{i+1})\dot{\tilde{x}}^{n+1}_- + \xi_{i+1}\dot{\tilde{x}}^{n+1}_+\right)\frac{V^n_{i+\frac{3}{2}}+V^n_{i+\frac{1}{2}}}{2} - \left[(1-\xi_i)\dot{\tilde{x}}^{n+1}_- + \xi_i\dot{\tilde{x}}^{n+1}_+\right]\frac{V^n_{i+\frac{1}{2}}+V^n_{i-\frac{1}{2}}}{2}}{\Delta\xi(\tilde{x}^n_+-\tilde{x}^n_-)} = 0,\\
&\mu^{n+1}_{i+\frac{1}{2}} = \frac{\kappa^{n+1}_{i+\frac{3}{2}} - 2\kappa^{n+1}_{i+\frac{1}{2}} + \kappa^{n+1}_{i-\frac{1}{2}}}{(\tilde{x}^n_+-\tilde{x}^n_-)^2(\Delta\xi)^2},\\
&\kappa^{n+1}_{i+\frac{1}{2}} = \frac{V^{n+1}_{i+\frac{3}{2}} - 2V^{n+1}_{i+\frac{1}{2}} + V^{n+1}_{i-\frac{1}{2}}}{(\tilde{x}^n_+-\tilde{x}^n_-)^3(\Delta\xi)^2}.
\end{aligned} \tag{B6}$$

After introducing the ghost points at $i+\frac{1}{2} = -\frac{1}{2}, N+\frac{1}{2}$, the boundary conditions are discretized using the average for the values of $(\tilde{h},\kappa,\mu)$ and the standard central difference stencil for their derivatives. In particular, the contact line velocities $\dot{\tilde{x}}^{n+1}_\pm$ are computed using the formulas

$$\dot{\tilde{x}}^{n+1}_- = -\frac{\left(\frac{V^n_{\frac{1}{2}}+V^n_{-\frac{1}{2}}}{2}\right)^2\left(\mu^{n+1}_{\frac{1}{2}}-\mu^{n+1}_{-\frac{1}{2}}\right)}{3\nu(\tilde{x}^n_+-\tilde{x}^n_-)^3\Delta\xi}, \quad \dot{\tilde{x}}^{n+1}_+ = -\frac{\left(\frac{V^n_{N+\frac{1}{2}}+V^n_{N-\frac{1}{2}}}{2}\right)^2\left(\mu^{n+1}_{N+\frac{1}{2}}-\mu^{n+1}_{N-\frac{1}{2}}\right)}{3\nu(\tilde{x}^n_+-\tilde{x}^n_-)^3\Delta\xi}. \tag{B7}$$

This algebraic system of equations is linear in the variables $V^{n+1}_{i+\frac{1}{2}}$, $\kappa^{n+1}_{i+\frac{1}{2}}$, $\mu^{n+1}_{i+\frac{1}{2}}$, $(K_0^\pm)^{n+1}$, $(K_1^\pm)^{n+1}$, and $\dot{\tilde{x}}^{n+1}_\pm$, including the ghost values. Therefore, it can be solved using a linear solver in each time step. In addition, by summing up the first equation in Eq. (B6) for all i and using Eq. (B7), it can be easily shown that this scheme conserves the volume in the sense that

$$\sum_{i=1}^{N} V_{i+\frac{1}{2}}^{n+1} = \sum_{i=1}^{N} V_{i+\frac{1}{2}}^{n}.$$

[1] R. Style, Y. Che, S. J. Park, B. M. Weon, J. H. Je, C. Hyland, G. K. German, M. P. Power, L. A. Wilen, J. S. Wettlaufer, and E. R. Dufresne, Patterning droplets with durotaxis, Proc. Natl. Acad. Sci. USA **110**, 12541 (2013).

[2] J. Bueno, Y. Bazilevs, R. Juanes, and H. Gomez, Droplet motion driven by tensotaxis, Extreme Mech. Lett. **13**, 10 (2017).

[3] L. Pieuchot, J. Marteau, A. Guignandon, T. Dos Santos, I. Brigaud, P.-F. Chauvy, T. Cloatre, A. Ponche, T. Petithory, P. Rougerie, M. Vassaux, J.-L. Milan, N. T. Wakhloo, A. Spangenberg, M. Bigerelle, and K. Anselme, Curvotaxis directs cell migration through cell-scale curvature landscapes, Nat. Commun. **9**, 3995 (2018).

[4] C. Neinhuis and W. Barthlott, Characterization and distribution of water-repellent, self-cleaning plant surfaces, Ann. Botany **79**, 667 (1997).

[5] T. Mouterde, G. Lehoucq, S. Xavier, A. Checco, C. Black, A. Rahman, T. Midavaine, C. Clanet, and D. Quéré, Antifogging abilities of model nanotextures, Nat. Mater. **16**, 658 (2017).

[6] Q. Wang, X. Yao, H. Liu, D. Quéré, and L. Jiang, Self-removal of condensed water on the legs of water striders, Proc. Natl. Acad. Sci. USA **112**, 9247 (2015).

[7] A. T. Bradley, F. Box, I. J. Hewitt, and D. Vella, Wettability-Independent Droplet Transport by Bendotaxis, Phys. Rev. Lett. **122**, 074503 (2019).

[8] A. T. Bradley, I. J. Hewitt, and D. Vella, Droplet trapping in bendotaxis caused by contact angle, Phys. Rev. Fluids **6**, 114003 (2021).

[9] R. Pericet-Cámara, A. Best, H.-J. Butt, and E. Bonaccurso, Effect of capillary pressure and surface tension on the deformation of elastic surfaces by sessile liquid microdrops, Langmuir **24**, 10565 (2008).

[10] Y. Xu, W. C. Engl, E. R. Jerison, K. J. Wallenstein, C. Hyland, L. A. Wilen, and E. R. Dufresne, Imaging in-plane and normal stresses near an interface crack using traction force microscopy, Proc. Natl. Acad. Sci. USA **107**, 14964 (2010).

[11] R. Roman and J. Bico, Elasto-capillarity: deforming an elastic structure with a liquid droplet, J. Phys.: Condens. Matter **22**, 493101 (2010).

[12] E. R. Jerison, Y. Xu, L. A. Wilen, and E. R. Dufresne, Deformation of an Elastic Substrate by a Three-Phase Contact Line, Phys. Rev. Lett. **106**, 186103 (2011).

[13] L. Limat, Straight contact lines on a soft, incompressible solid, Eur. Phys. J. E **35**, 134 (2012).

[14] A. Marchand, S. Das, J. H. Snoeijer, and B. Andreotti, Contact Angles on a Soft Solid: From Young's Law to Neumann's Law, Phys. Rev. Lett. **109**, 236101 (2012).

[15] R. W. Style, R. Boltyanskiy, Y. Che, J. S. Wettlaufer, L. A. Wilen, and E. R. Dufresne, Universal Deformation of Soft Substrates Near a Contact Line and the Direct Measurement of Solid Surface Stresses, Phys. Rev. Lett. **110**, 066103 (2013).

[16] T. Kajiya, A. Daerr, T. Narita, L. Royon, F. Lequeux, and L. Limat, Advancing liquid contact line on viscoelastic gel substrates: Stick-slip vs. continuous motions, Soft Matter **9**, 454 (2013).

[17] L. A. Lubbers, J. H. Weijs, L. Botto, S. Das, B. Andreotti, and J. H. Snoeijer, Drops on soft solids: free energy and double transition of contact angles, J. Fluid Mech. **747**, R1 (2014).

[18] R. W. Style and E. R. Dufresne, Static wetting on deformable substrates, from liquids to soft solids, Soft Matter **8**, 7177 (2012).

[19] R. W. Style, A. Jagota, C.-Y. Hui, and E. R. Dufresne, Elastocapillarity: Surface tension and the mechanics of soft solids, Annu. Rev. Condens. Matter Phys. **8**, 99 (2017).

[20] Z. Zhang, J. Yao, and W. Ren, Static interface profiles for contact lines on an elastic membrane with the Willmore energy, Phys. Rev. E **102**, 062803 (2020).

[21] T. Young, An essay on the cohesion of fluids, Philos. Trans. R. Soc. London **95**, 65 (1805).
[22] C. Huh and L. Scriven, Hydrodynamic model of steady movement of a solid/liquid/fluid contact line, J. Colloid Interface Sci. **35**, 85 (1971).
[23] P.-G. De Gennes, Wetting: Statics and dynamics, Rev. Mod. Phys. **57**, 827 (1985).
[24] D. Bonn, J. Eggers, J. Indekeu, J. Meunier, and E. Rolley, Wetting and spreading, Rev. Mod. Phys. **81**, 739 (2009).
[25] S. R. De Groot and P. Mazur, *Nonequilibrium Thermodynamics* (Courier Corporation, Boston, MA, 2013)
[26] L. Onsager, Reciprocal relations in irreversible processes, part I, Phys. Rev. **37**, 405 (1931).
[27] L. Onsager, Reciprocal relations in irreversible processes part II, Phys. Rev. **38**, 2265 (1931).
[28] M. Doi, Onsager variational principle in soft matter dynamics, in *Non-Equilibrium Soft Matter Physics* (World Scientific, Singapore, 2012), pp. 1–35.
[29] T. Qian, X.-P. Wang, and P. Sheng, A variational approach to moving contact line hydrodynamics, J. Fluid Mech. **564**, 333 (2006).
[30] X. Xu, U. Thiele, and T. Qian, A variational approach to thin film hydrodynamics of binary mixtures, J. Phys.: Condens. Matter **27**, 085005 (2015).
[31] U. Thiele, A. J. Archer, and L. M. Pismen, Gradient dynamics models for liquid films with soluble surfactant, Phys. Rev. Fluids **1**, 083903 (2016).
[32] M. Doi, Onsager principle as a tool for approximation, Chin. Phys. B **24**, 020505 (2015).
[33] X. Xu, Y. Di, and M. Doi, Variational method for contact line problems in sliding liquids, Phys. Fluids **28**, 087101 (2016).
[34] X. Man and M. Doi, Ring to Mountain Transition in Deposition Pattern of Drying Droplets, Phys. Rev. Lett. **116**, 066101 (2016).
[35] M. C. Marchetti, J.-F. Joanny, S. Ramaswamy, T. B. Liverpool, J. Prost, M. Rao, and R. A. Simha, Hydrodynamics of soft active matter, Rev. Mod. Phys. **85**, 1143 (2013).
[36] F. Jülicher, S. W. Grill, and G. Salbreux, Hydrodynamic theory of active matter, Rep. Prog. Phys. **81**, 076601 (2018).
[37] C. Bechinger, R. Di Leonardo, H. Löwen, C. Reichhardt, G. Volpe, and G. Volpe, Active particles in complex and crowded environments, Rev. Mod. Phys. **88**, 045006 (2016).
[38] J.-F. Joanny and S. Ramaswamy, A drop of active matter, J. Fluid Mech. **705**, 46 (2012).
[39] A. Loisy, J. Eggers, and T. B. Liverpool, Tractionless Self-Propulsion of Active Drops, Phys. Rev. Lett. **123**, 248006 (2019).
[40] S. Trinschek, F. Stegemerten, K. John, and U. Thiele, Thin-film modeling of resting and moving active droplets, Phys. Rev. E **101**, 062802 (2020).
[41] H. Wang, T. Qian, and X. Xu, Onsager's variational principle in active soft matter, Soft Matter **17**, 3634 (2021).
[42] W. Helfrich, Elastic properties of lipid bilayers: Theory and possible experiments, Z. Naturforsch. C **28**, 693 (1973).
[43] T. Qian, X.-P. Wang, and P. Sheng, Molecular scale contact line hydrodynamics of immiscible flows, Phys. Rev. E **68**, 016306 (2003).
[44] T. Qian, X.-P. Wang, and P. Sheng, Power-Law Slip Profile of the Moving Contact Line in Two-Phase Immiscible Flows, Phys. Rev. Lett. **93**, 094501 (2004).
[45] E. Tjhung, D. Marenduzzo, and M. E. Cates, Spontaneous symmetry breaking in active droplets provides a generic route to motility, Proc. Natl. Acad. Sci. USA **109**, 12381 (2012).
[46] Z. Zhang, S. Xu, and W. Ren, Derivation of a continuum model and the energy law for moving contact lines with insoluble surfactants, Phys. Fluids **26**, 062103 (2014).